2021

Modeling Stromatolite Formation with Diffusion-Limited Aggregation

Laura E. Stevens
The University Of Montana

MODELING STROMATOLITE FORMATION WITH DIFFUSION-LIMITED AGGREGATION

By

LAURA ELIZABETH STEVENS

B.S., Astrophysics, Physics, and Biology, College of Charleston, Charleston, SC, 2013

Thesis presented in partial fulfillment of the requirements for the degree of Master of Science in Geosciences

The University of Montana
Missoula, MT

Spring 2021

Approved by:

Scott Whittenburg, Dean of The Graduate School
Graduate School

Nancy Hinman, Committee Chair
Department of Geosciences

Hilary Martens, Committee Co-Chair
Department of Geosciences

Jesse Johnson, Committee Co-Chair
Department of Computer Science

Stevens, Laura, M.S., Spring 2021 Geosciences

Modeling Stromatolite Formation with Diffusion-Limited Aggregation

Committee chair: Dr. Nancy Hinman

Stromatolites, microbialites, and other microbially induced sedimentary structures exist in the rock record as far back as 3.6 billion years ago and continue to form in the present day. Better characterizing these structures and better understanding how they form is crucial in distinguishing these biosignatures from similar, abiotic structures, which can help us to understand the conditions of early Earth and early Mars. To that end, I have modified *DLA 3D EXT*, an open-source stromatolite modeling program, to more closely reflect the process of microbial trapping-and-binding by filamentous microbes in a calcite-precipitating hot spring system. This modified program includes a field of upright spikes that can trap incoming particles and sediment. I simulated stromatolites forming with different spike heights, spike spacings, and stickiness. To quantify these stromatolites' morphologies, I obtained the fractal dimension and lacunarity of a section of each resulting structure. I found that stickiness affects morphology as measured by both fractal dimension and lacunarity. This may help us better distinguish true stromatolites from abiotic imposters.

Acknowledgments

I would like to express my deep gratitude to my entire committee for their sharing their knowledge and insight with me over many, many Zoom meetings. This is a weird time to do anything other than cower indoors, so thank you to everyone for adapting. I'd especially like to thank Hilary for helping me develop and stick to a schedule (it didn't work, but thank you for trying), and Nancy for being an outstanding advisor!

I'd also like to thank Marco Maneta for helping me get started compiling software in Eclipse, Eric Verrecchia for providing me with *DLA 3D EXT*, and Damien Chappatte for writing *DLA 3D EXT*.

Finally, thank you to my multiple therapists and Mark Reiser for your professional emotional support. And thank you to my partner Ryan, my mother, and my sister, for your non-professional emotional support and for helping me have a sense of home and belonging in these weird times.

Contents

List of Figures

List of Tables

Chapter 1: Introduction

1.1: The Problem: Biosignature Validation

In Februrary of 2021, the Perseverance rover landed on Mars. It is currently exploring Jezero Crater, the remains of an ancient river delta, full of hydrated minerals [*Mangold et al.*, 2020]. Curiosity is also working on Mars, exploring the remains of an ancient lakebed in Gale Crater [*Grotzinger et al.*, 2015]. And both Spirit and Mars Reconnaissance Orbiter discovered several deposits of hydrated minerals and sinters in Gusev Crater, indicating extinct hot springs [*Ruff et al.*, 2020]. If life ever existed on Mars, these sites are all excellent places to look. But what would we expect to find there?

The Martian atmosphere thinned very rapidly, reaching its current thickness some 600 million years after formation [*Mahaffy et al.*, 2013]. This would also cause rapid water loss, meaning Mars has been dry for some time. If life ever existed on Mars, it is unlikely to have become more complex than unicellular organisms. This means that astrobiological missions to Mars are looking for the traces of microbial life, which is an exciting and challenging problem for both astrobiologists and early-Earth paleontologists.

Microbial life leaves behind traces in the rock record, but these can be very difficult to verify. One famous example is the Martian meteorite ALH-84001, in which nanoscale filaments that resembled microbes were found and suggested to be microfossils [*McKay et al.*, 1996]. Consensus appears to suggest that they were, instead, abiotically produced, highlighting the need to establish clear criteria for biosignatures, especially of microbial life [*Brasier and Wacey*, 2012].

One of the more recent attempts at this comes from *Neveu et al.* [2018], who propose a "ladder of life detection" based on seven criteria: detections must be sensitive, contamination-free, repeatable, detectable, survivable, reliable, compatible with current definitions of life, and a last-resort hypothesis—that is, a particular detection can be ascribed to life only if all other explanations have been exhausted. The ladder ascends from the least to most essential qualities of life, each relying on the rung below it (figure 1.1).

While being named the ladder of life detection, not everything in the ladder is a biosignature. At the top of the ladder is Darwinian evolution. It is not a biosignature, and often not even detectable, because it is a process. Biosignatures can record snapshots of the evolutionary process and were (and are) integral to developing the theory. But observing evolution without having observed life is a cart-before-the-horse scenario: it is necessary to establish that living things exist before observing how those living things change over time.

At the bottom of the ladder are biofabrics, the textures and structures from microbial communities that can be preserved in rock. Biofabrics are broadly described as microbially

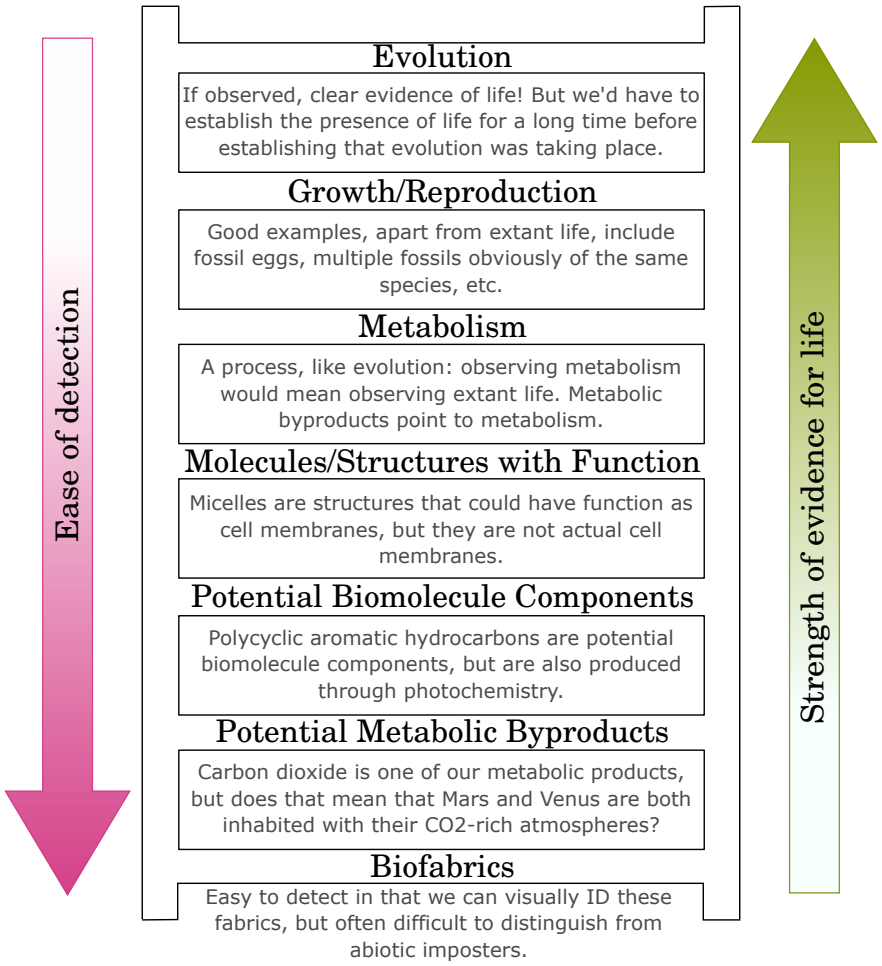

Figure 1.1: The ladder of life detection, adapted from [*Neveu et al.*, 2018]. Some elaboration for each ladder run is provided. Biofabrics such as stromatolites are right at the bottom: easy to detect but hard to demonstrate as products of life.

induced sedimentary structures (MISS). MISS include structures—such as level bedding surfaces, spongy pore fabrics, and multidirectional ripple marks—that formed as incoming sediment and particles interacted with microbial mats on sandy surfaces [*Noffke et al.*, 2001]. MISS also include stromatolites, the least disputed fossils of microbes: upward-projecting layered rock structures, typically in domes, cones, and branches. Both MISS and stromatolites can form as microbial mats trap and bind incoming sediment and particles (figure 1.2). Stromatolites exist in the rock record as early as 3.6 Ga [*Grotzinger and Knoll*, 1999], and many currently form as microbes trap and bind sediments. Therefore, ancient stromatolites are thought to have formed the same way.

But while stromatolites are the least disputed fossils of microbes, they are still at the bottom of the ladder, because morphology is not necessarily enough to demonstrate biogenicity. A complete fossil skeleton of a vertebrate is one thing, but layered rock is quite another.

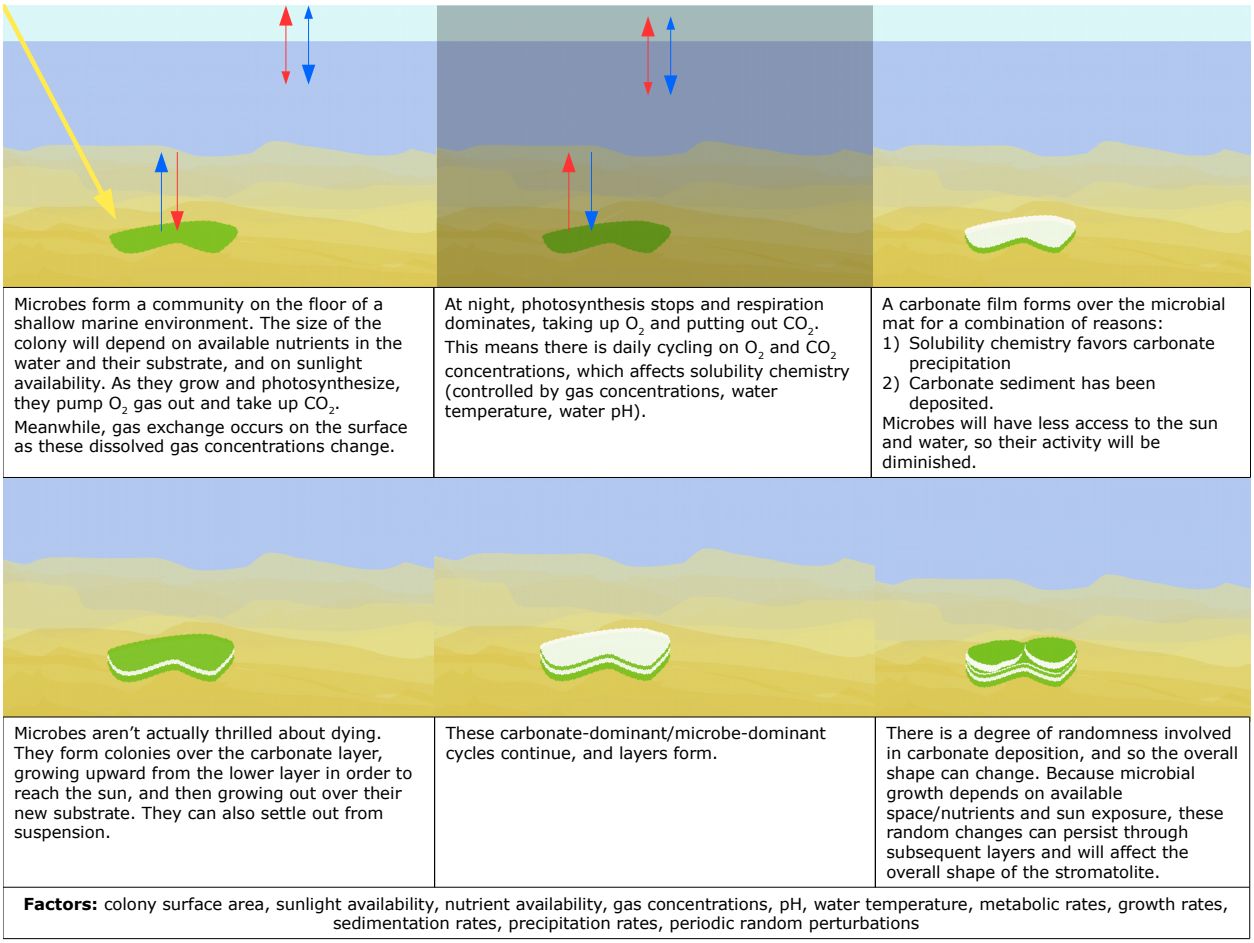

Figure 1.2: Biological stromatolite formation. Yellow arrow: light; red arrows: CO_2, blue arrows: O_2.

Stromatolites form cones, domes, and branches; however, so do many abiotic structures. Aragonite, for example, forms branching needles under the right conditions, and many abiotic speleothems are also layered cones, domes, and branches (figure 1.3) [*Self and Hill*, 2003]. To further complicate matters, these examples are all made of the same thing. Precambrian stromatolites are overwhelmingly composed of calcium carbonate; therefore, being able to reliably distinguish them from similar abiotic calcite structures is an even more difficult task. This makes satisfying the "explanation of last resort" criterion of *Neveu et al.* [2018] quite a thorny problem.

A possible advantage of the carbonate composition of all these structures is that, hypothetically, isotopic analysis can help to determine whether a particular stromatolite-like structure is actually a stromatolite. Carbon fixation through photosynthesis strongly favors fixing carbon-12 over carbon-13, in large excess of abiotic chemical reactions. This is because carbon-12 requires less energy to fix and because metabolic reactions frequently do not go to completion, making it less likely that the reaction would reach a point where it used heavier isotopes [*White*, 2013]. Therefore, samples of graphite, carbonates, or kerogens containing

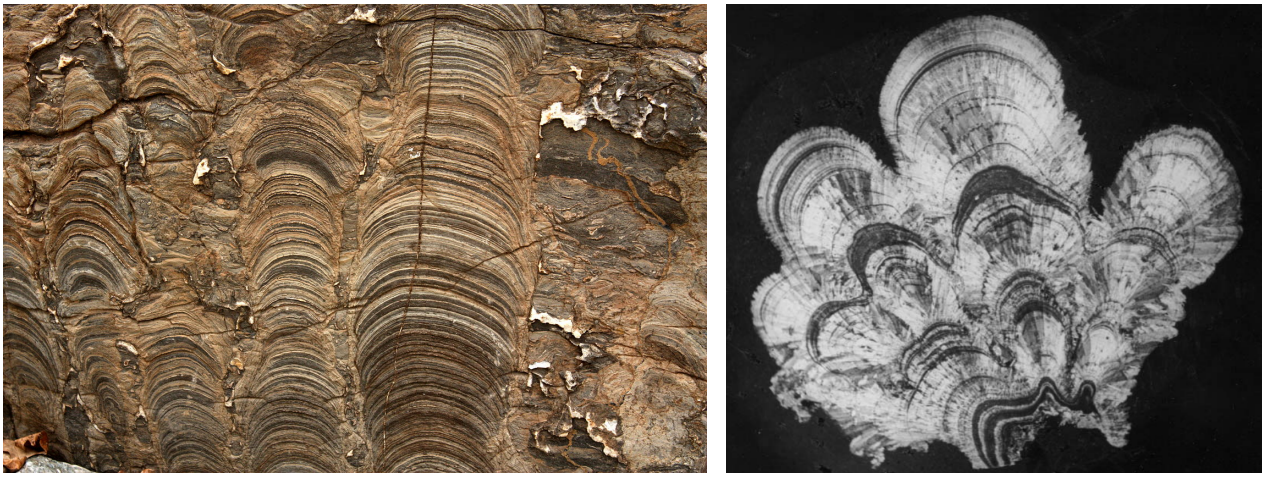

(a) **(b)**

Figure 1.3: Cross-sections of a stromatolite (a) and a coralloid (b).

abnormally high ^{12}C relative to ^{13}C are considered biosignatures and have been used to establish an origin of life around 3.8 Ga [*Mojzsis et al.*, 1996; *Schidlowski*, 1988].

But even if isotopic analysis can clearly demonstrate the biogenicity of a layered rock structure, fulfilling that "last resort" criterion, that really only scratches the surface of what could be interesting about it. Stromatolites provide a window into long-extinct taxa representing the earliest cellular life. Their morphologies may reflect that life, although it is important to include the usual caveat tied to all ancient rocks; that is, diagenetic processes can erase and confound any and all types of data, be they morphological, isotopic, or compositional. But all surviving data helps to build a picture of some of our oldest ancestors, and the more accurately we can interpret those data, the more complete that picture will be.

If there is a clear morphological difference between stromatolites and similar, abiotic structures, that can be exploited to accurately identify biosignatures, which is currently a very difficult task. Specifically, it is unknown which properties of a microbial mat may be reflected in stromatolite morphology; therefore, this work investigates whether three specific properties—attraction radius, microbe filament height, and filament spacing—have an effect on stromatolite morphology. Results from *Dupraz et al.* [2006] suggest that attraction radius, which can be thought of as how sticky a microbial mat is, produces more clustered structures. And historically, stromatolites have been assumed to have structures unique to the microbes that produced it, with some researchers going so far as to give stromatolite genus names (e.g. *Donaldson* [1976]). So it is expected that attraction radius, filament height, and filament spacing will all have an effect on stromatolite morphology.

To answer this question, I used *DLA 3D EXT*, an open-source stromatolite formation simulator [*Chappatte*, 2010], to simulate stromatolites forming over spiky starting surfaces, approximating a mat of filamentous microbes. I manipulated the height and spacing of the spikes to mimic different microbial morphologies. I also manipulated the attraction radius,

which is the distance a particle must come to a growth surface in order to attach, to mimic the production of EPS. The simulations were run using the travertine-depositing springs at Yellowstone National Park as a natural basis and the ranges for each variable were chosen accordingly. Cross sections from the resulting structures were then run through fractal analysis software, which allowed me to quantify the structures' morphologies. For each cross section, I obtained the fractal dimension, which quantifies how clustered a structure is, and the lacunarity, which quantifies the distribution of gaps in a structure. By graphing these fractal properties against the range of values used for each variable, I was able to see whether mat morphology or attraction radius influenced the final structure in a measurable way.

These results will provide insight into which properties of microbial mats most strongly influence stromatolite morphology. It will also help improve methods for assessing the validity of proposed stromatolites. Potentially, the relationships between the properties of microbial mats and the stromatolites they produce can be applied to any layered rock structure and, coupled with methods such as isotope analysis, can make assessments of these structures as biosignatures more robust and reliable. Furthermore, the fractal analysis used here can be applied to images of natural stromatolites to build a database of stromatolite characteristics and dimensions, which would be a valuable resource to astrobiologists.

1.2: How Do Stromatolites Grow?

1.2.1: Physical Processes

As mentioned before, the primary model for calcite stromatolite formation, and the formation of some other MISS, is the trapping-and-binding mechanism, illustrated in figure 1.4. An initial microbial mat forms on a solid surface beneath water. As sediment washes in and particles fall out of solution, the microbes trap all that detritus around them. Often, these microbes are filamentous and particles get tangled up in the thicket of microbe bodies. Furthermore, all microbes exude extracellular polymeric substances (EPS). EPS has many functions, from defense against entombment to aiding in cell-to-cell chemical communication within the mat [*Frederick et al.*, 2011]. For stromatolite formation, EPS is important for two reasons: (1) because it is sticky, providing another way to trap sediment and particles and (2) because it protects against entombment by moving trapped particles outward and away from the cell exuding it [*Arp et al.*, 1999], which could create shapes that qualify as MISS.

As the mat continues to accumulate particles, those particles create a new substrate for microbes to occupy. Stromatolite-forming microbes are typically photosynthetic, so they need access to sunlight and therefore grow upward. Over time, a stack of alternating microbe-sediment layers forms, and over a long time, the lower tiers of microbes die and the sediment lithifies, producing a layered rock structure that may contain microbial casts or organic molecules.

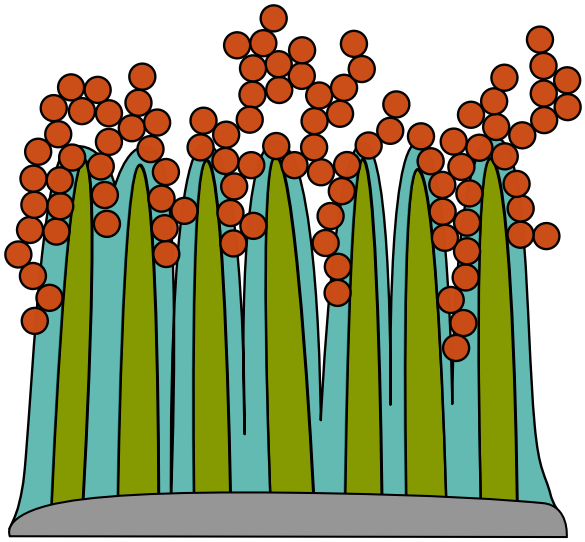

Figure 1.4: Trapping and binding mechanism for stromatolite formation. Photosynthetic microbes (green) exude extracellular polymeric substances (EPS, blue) to protect from incoming sediment (orange) and communicate with other cells. Sediment is trapped by the microbial filaments and the EPS.

1.2.2: Chemical Processes

The inorganic components of a stromatolite can have any composition, depending on the environment of formation. This work focuses on carbonate stromatolites, which are intimately tied up with biochemistry through the processes of photosynthesis and respiration. A detailed overview of carbonate chemistry and how it relates to stromatolite formation can be found in appendix A; here is a brief overview.

The reaction governing calcite precipitation and dissolution is

$$\mathrm{CaCO_3 + H_2CO_3 \rightleftharpoons Ca^{2+} + 2\,HCO_3^-}. \tag{1.1}$$

The left-hand side (LHS) of the equation starts with calcite and carbonic acid: the products of precipitation. The right-hand side (RHS) shows calcium ions and bicarbonate: the products of dissolution.

Atmosphering CO_2 concentration also plays a role: when CO_2 dissolves into water, they react to produce carbonic acid, which dissociates to produce bicarbonate and carbonate:

$$\mathrm{CO_2 + H_2O \rightleftharpoons HCO_3^- + H^+ \rightleftharpoons CO_3^{2-} + 2\,H^+} \tag{1.2}$$

According to Le Chatelier's principle, the amount of reactants (i.e., species on the LHS of

a chemical equation) vs. the amount of products (i.e. species on the RHS) can drive a reversible solubility reaction in either direction in an effort to achieve energetic equilibrium. More reactants drives the reaction to the right, creating more products until equilibrium is reached. Similarly, more products drive the reaction to the left, destroying product to form more reactants.

This means that as atmospheric CO_2 dissolves into water to create carbonic acid, the amount of H_2CO_3 on the LHS of equation 1.1 increases, driving the reaction toward dissolution.

While Le Chatelier's principle describes the effects of concentration on solubility, van 't Hoff's equation describes the effects of temperature. At standard atmospheric pressure (a fair enough assumption in most MISS-forming environments), van 't Hoff's equation is

$$\frac{d}{dT} \ln K_{eq} = \frac{\Delta H^{\Theta}}{RT^2}, \tag{1.3}$$

where T is temperature, K_{eq} is the solubility constant of the species at equilibrium, ΔH^{Θ} is the enthalpy of reaction (constant at constant pressure), and R is the ideal gas constant.

This work assumes a constant rate of calcite precipitation, which applies when pressure/temperature conditions are constant and solution composition is fairly stable. This assumption is reasonable for the hot-springs system that provides the natural analog for this work (see section 2.1.1). Table 1.1 summarizes only the abiotic factors in a hot spring system, while table 1.2 summarizes how microbes affect and are affected by those abiotic factors.

Table 1.1: Breakdown of chemical aspects of stromatolite formation in a hot spring system. In this model, water temperature, atmospheric pressure, and pH are treated as constant.

System Part	***Depends on ...***	***Affects ...***
Water temperature	Geothermal heating	Gas solubility
Atmospheric composition and pressure	Temperature, elevation, local pollution, local organisms	Temperature, gas solubility
Gas solubility	Van 't Hoff, Henry's law, Law of Mass Action	pH, calcite solubility
pH	Van 't Hoff, Law of Mass Action	Calcite solubility
Calcite solubility → precipitation rate	Van 't Hoff, Law of Mass Action	Surface growth

Table 1.2: Breakdown of biotic and abiotic relationships contributing to stromatolite formation in a hot spring system. This work focuses on the bottom row.

System Part	***Effects on microbes***	***Effects from microbes***
Water temperature	Defines zones of habitability	None
Atmospheric composition and pressure	Habitability, nutrient availability	Metabolic products enter atmosphere.
Gas solubility	Habitability, nutrient availability	Take in and produce gases (usually CO_2 and O_2).
pH	Habitability, water chemistry	Take in and produce acids, bases, buffers.
Calcite solubility $\rightarrow$ precipitation rate	New substrates for growth, possible entombment	Effects on aqueous geochem drive solubility reactions, EPS and microbe/mat shape influence surface shape.

1.3: Modeling As a Way to Understand Stromatolites

1.3.1: 2D Modeling

Abiotic stromatolite growth was explored by *Grotzinger and Rothman* [1996] when they built a numerical model using the Kardar-Parisi-Zhang (KPZ) equation [*Kardar et al.*, 1986], which describes how a height field over some horizontal space changes over time using the equation

$$\frac{\partial h(\vec{x},t)}{\partial t} = \nu\nabla^2 h + \frac{\lambda}{2}(\nabla h)^2 + \eta(\vec{x},t), \tag{1.4}$$

where h is layer height, $\vec{x}$ is horizontal position, t is time, ν and λ are parameters, and $\eta(\vec{x},t)$ is noise.

The KPZ equation provides some room for tailoring and modification depending on how ν, λ, and $\eta(\vec{x},t)$ are defined and therefore is used to model everything from silica deposition to tumor growth. The equation as *Grotzinger and Rothman* [1996] used it is

$$\frac{\partial h}{\partial z} = v_s + \kappa\nabla^2 h + v_p\sqrt{1+(\nabla h)^2} + \eta(x,t), \tag{1.5}$$

where h is layer thickness, v_s is the rate of upward growth from sedimentation, κ is the rate of diffusion, v_p is rate of upward growth from precipitation, and $\eta(x,t)$ is noise.

Grotzinger and Rothman [1996] found that their abiotic model yielded structures very similar to stromatolites, suggesting that not every structure identified as a stromatolite was actually biogenic. Since that model was reported, other stromatolite models based on the KPZ equation have been carried out. Some results support the conclusions of *Grotzinger and Rothman* [1996] and some refute them (e.g. *Batchelor et al.* [2004]), depending on how ν and λ are defined.

Cuerno et al. [2012] conducted a metastudy of KPZ stromatolite models and concluded that the method has some flaws. How ν and λ are defined often involves a lot of simplifying assumptions about a stromatolite-forming system and ultimately may just reflect how optimistic a modeler is about the biogenicity of a layered structure.

Figure 1.5: Stromatolite from the 2.7 Ga Tumbiana formation with arrow indicating overhang, from *Cuerno et al.* [2012].

Futhermore, some structures, such as dome stromatolites with overhang (figure 1.5) were not able to be replicated by any KPZ model, regardless of whether the authors concluded that all structures believed to be stromatolites are indeed biogenic. This means that the equation may have some important limitations and other approaches should be explored.

Diffusion-limited aggregation (DLA) and cellular automata (CA) algorithms are appealing alternatives to KPZ. The KPZ implementation in *Grotzinger and Rothman* [1996], while modified to reflect the film-accumulation process, does not actually *replicate* the process. However, DLA replicates particles accumulating into films and so more directly mirrors the system under inquiry. DLA starts with a field full of particles and a designated starting growth surface called a seed point (which can be any shape). When particles contact the growth surface, they attach and become part of the growth surface. The result are the dendritic structures seen in figure 1.6.

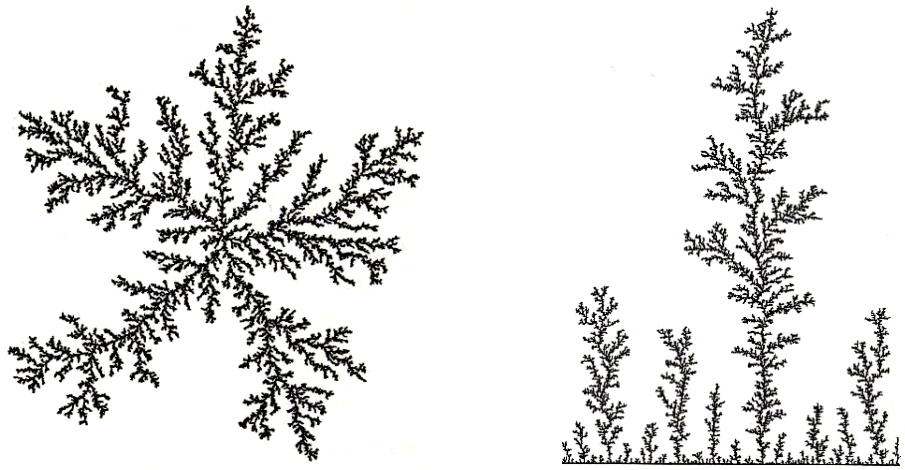

(a) **(b)**

Figure 1.6: Structures created by DLA, using (a) a central seed point and (b) a seed line, from [*Feder*, 1988, pp. 34, 56].

Dupraz et al. [2006] applied DLA and CA in their own stromatolite model, which both confirmed the results of *Grotzinger and Rothman* [1996] and was able to replicate some stromatolite structures that KPZ models could not, including steep slopes and overhang (figure 1.7). The work done by *Dupraz et al.* [2006] provided the foundation for *DLA 3D EXT*, which uses the same algorithms translated to three dimensions.

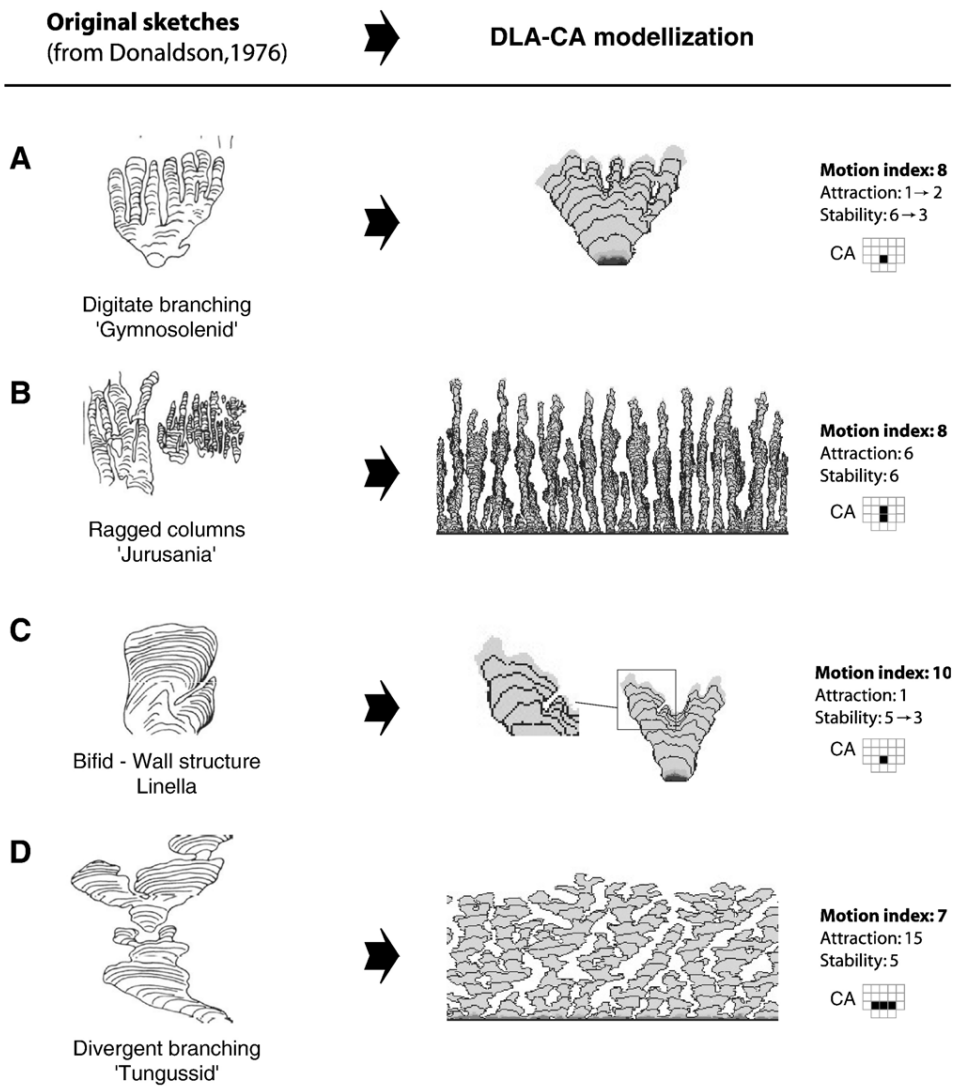

Figure 1.7: Figure from *Dupraz et al.* [2006], comparing modeled structures to known stromatolites from *Donaldson* [1976].

1.3.2: 3D Modeling with *DLA 3D EXT*

DLA 3D EXT [*Chappatte*, 2010] extends the algorithms used by *Dupraz et al.* [2006] into three dimensions. The model does not reflect explicitly abiotic or biotic processes; rather, output can be interpreted to represent one or both. Algorithm 1 summarizes the process: particles, presumed to be calcite, move randomly above a surface; when they come within a certain distance of the surface (the attraction radius, or AR), they stop moving randomly, take the shortest path to the growth surface, and attach themselves. Sedimentation is also supported. Instead of moving with Brownian motion, sediment particles just fall straight down and settle into place.

Algorithm 1: Algorithm describing *DLA 3D EXT* .

```
Data: initial surface shape, attraction radius, particle size, particle abundance
Result: new surface shape
for each particle do
    while unattached to surface do
        if calcite particle then
            Brownian motion;
            if distance from surface <= attraction radius then
                fall straight in;
                attach to surface;
            end
        end
        else # otherwise particle is sediment, gravity dominates motion
            fall straight down
        end
        ;
    end
end
```

It is important to note that algorithm 1 describes the physical processes that the software is supposed to mimic. However, there are some discrepancies between the algorithm *Chappatte* [2010] claimed to implement and the actual implementation that will be addressed in the discussion.

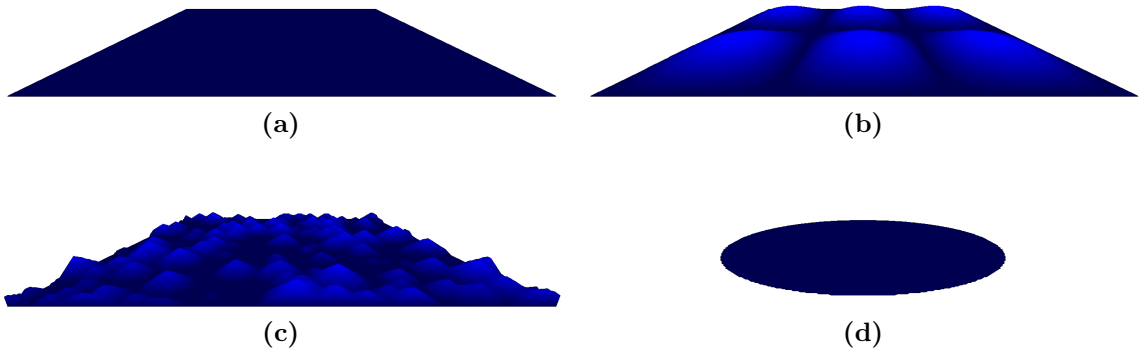

Figure 1.8: Available starting surfaces in *DLA 3D EXT*: (a) flat square, (b) sinusoidal, (c) random, (d) flat disk. From *Chappatte* [2010].

DLA 3D EXT has four initial surface configurations: flat square, sinusoidal, random roughness, and flat disk (figure 1.8). The flat surfaces can be interpreted as smooth rock, the sinusoidal surface as ripple marks or smooth river pebbles; the randomly rough surface as sand. But many of the microbes involved in stromatolite formation are filamentous, forming

a mat of spikes on which particles can accumulate. Because *DLA 3D EXT* is open-source, it can be modified to include such a surface.

1.4: Fractal Analysis

Fractals are shapes that have some self-repeating quality to them. Some of the common examples are abstract mathematical shapes like the Mandelbrot set and the Julia set (figure 1.9). In each, there are repeating subunits: in the Mandelbrot set, there are circles ringing circles; in the Julia set, there are swirls of circles.

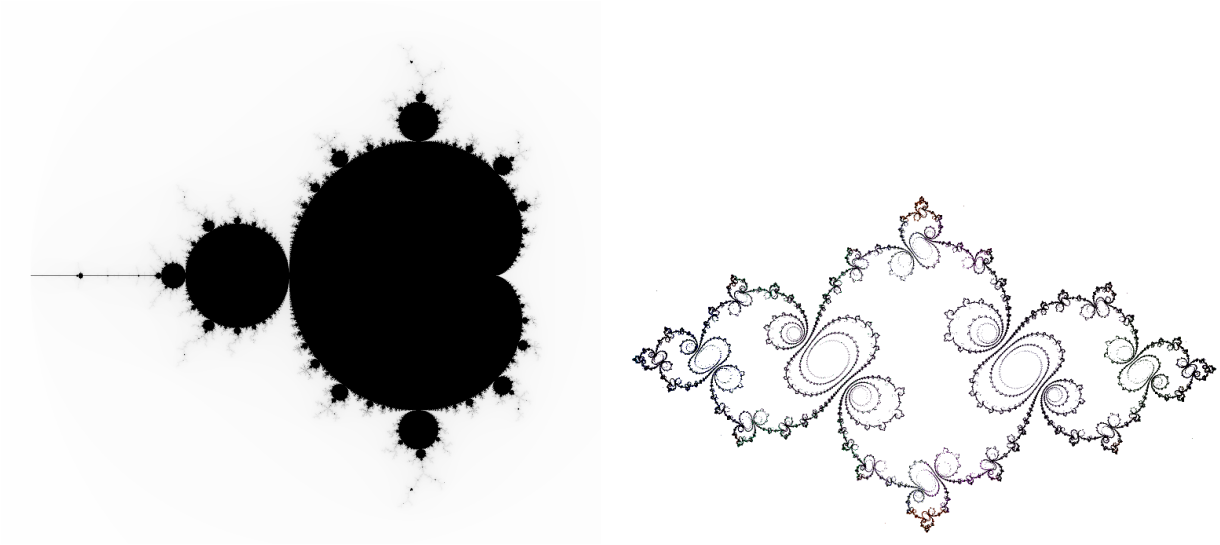

(a) **(b)**

Figure 1.9: Mandelbrot (a) and Julia (b) sets, common examples of fractal geometry.

In [*Feder*, 1988, p.11], Mandelbrot defines fractals generally as any shape that has a self-repeating characteristic to it. Fractals can also be defined as shapes that have fractional dimension. This is one of the main distinctions between Euclidean and fractal geometry: Euclidean geometry operates in integer dimensions, while fractal geometry operates in between (figure 1.10).

Many natural objects and phenomena are fractal, including stromatolites. *Hofmann* [1994] proposed using stromatolites' fractal dimension to characterize them and it is now a common quantitative way to approach stromatolites (e.g. *Grotzinger and Rothman* [1996]; *Verrecchia* [1996]). Fractal dimension can be found using the box counting algorithm, illustrated in figure 1.11.

There are two ways to conceptualize fractal dimension. One is how much of the next Euclidean dimension is filled: for example, if a shape has fractal dimension is between 1 and 2,

Figure 1.10: Euclidean vs. fractal dimension. Examples of fractals in the natural world are included.

it fills a certain amount of a 2D bounding shape. Fractal dimension can also be thought of as a measure of "clusteredness," with lower fractal dimension corresponding to more clustering.

Lacunarity is another property of fractals. It measures both rotational symmetry and the amount of empty space in a fractal shape—essentially, how "gappy" it is. In that sense, it is sort of an inverse of fractal dimension; however, fractal dimension does not include rotational symmetry, so they are not perfect complements. The smallest possible lacunarity is 0, which means a structure is perfectly rotationally invariant; however, lacunarity can be larger than 1. Lacunarity can also be found using the box-counting algorithm; whereas fractal dimension is found by counting the fully occupied boxes in a grid, lacunarity is found by counting how many occupied pixels are in each box [*Smith Jr et al.*, 1996].

Lacunarity is often overlooked in fractal analysis, possibly in part because it is often glossed over in texts and scientists using fractal analysis are usually teaching themselves on the

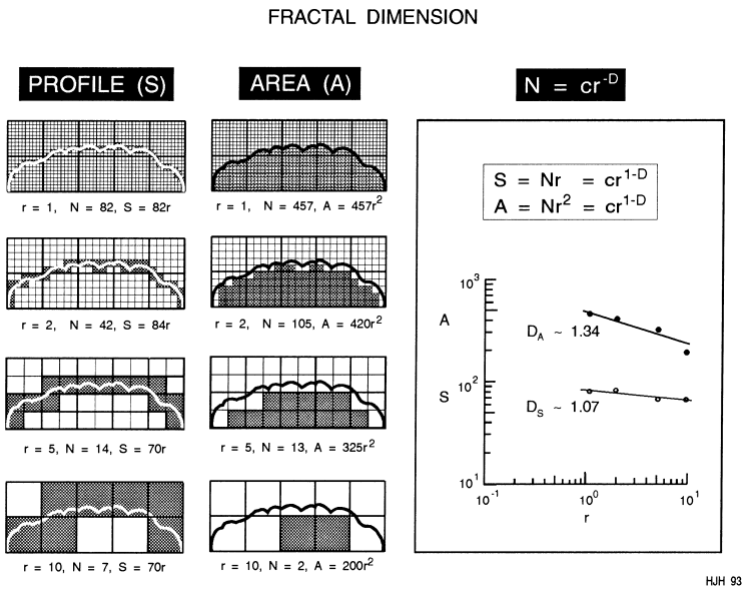

Figure 1.11: The box-count algorithm for finding fractal dimension, as illustrated in *Hofmann* [1994].

job. But because it is not the perfect inverse of fractal dimension, it could potentially be a useful way to quantify stromatolite morphology. In order to investigate that possibility, both fractal dimension and lacunarity were obtained for each simulated structure.

Chapter 2: Methods

2.1: Overview

2.1.1: The Natural System: Mammoth Hot Springs at Yellowstone National Park

This work uses Angel Terrace at Mammoth Hot Springs in Yellowstone National Park as its natural basis. Along with the rest of the springs at Mammoth, Angel Terrace deposits travertine and is located in the northwest corner of the park (figure 2.1). Its chemistry and depositional facies are very well characterized, with a detailed facies model developed by *Fouke et al.* [2000] (figure 2.2). *Calothrix* mats grow in the distal slope facies of Angel Terraace (figure 2.2), in temperatures ranging from 15–40 °C. Calcite particles in these waters range in size from 25–100 μm, with the smallest sizes corresponding to the lowest temperatures [*Farmer*, 2000; *Fouke et al.*, 2000].

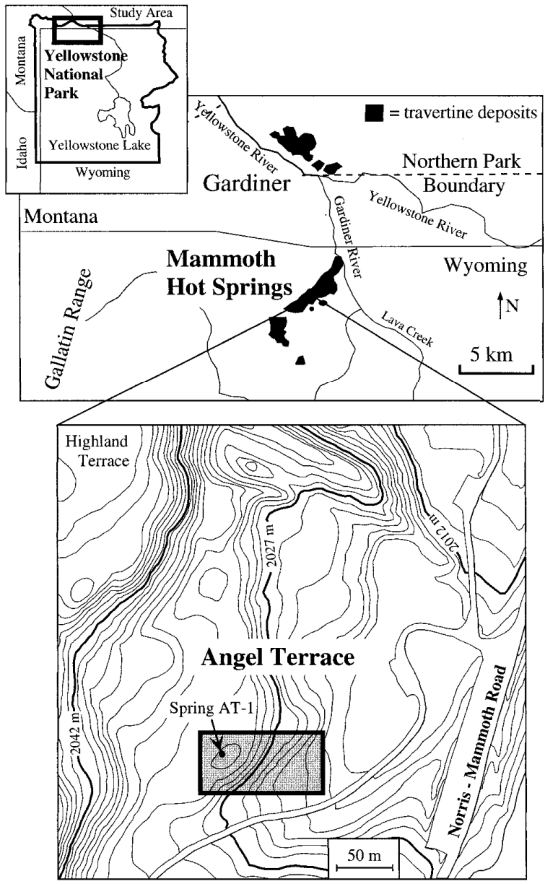

Figure 2.1: Angel Terrace's location within Mammoth Hot Springs. From *Fouke et al.* [2000].

The nature of this environment allows for certain assumptions to be made when modeling. There is little to no sediment coming into these springs, so sedimentation can be ignored. Because *Fouke et al.* [2000] found that *Calothrix* in Angel Terrace did not appreciably affect the rate of calcite precipitation, precipitation and attachment rates do not need to take into account day/night cycling or the fact that EPS can act as a calcite reservoir.

The *Calothrix* in Angel Terrace, and indeed most mentions of *Calothrix* in Yellowstone-related literature, are described only as *Calothrix spp.*, meaning that multiple species are present but no further characterization has been done. *Calothrix* morphologies have the same general plan: a nitrogen-fixing heterocyst at the base of the cell, a long tapering filament, often with a small hair at the end (see figure 2.3a). The filament is sheathed by EPS [*Hugo et al.*, 2011]. But the length and thickness of the filament, along with the thickness of the sheath, vary widely from species to species

(e.g. *Amand et al.* [2005]; *Norris and Castenholz* [2005]; *Uher* [2007]).

I used what is known about the physical and geochemical conditions at Angel Terrace and what is known about *Calothrix* to guide my investigation of the three variables of interest in my work: spike height, spike spacing, and attraction radius.

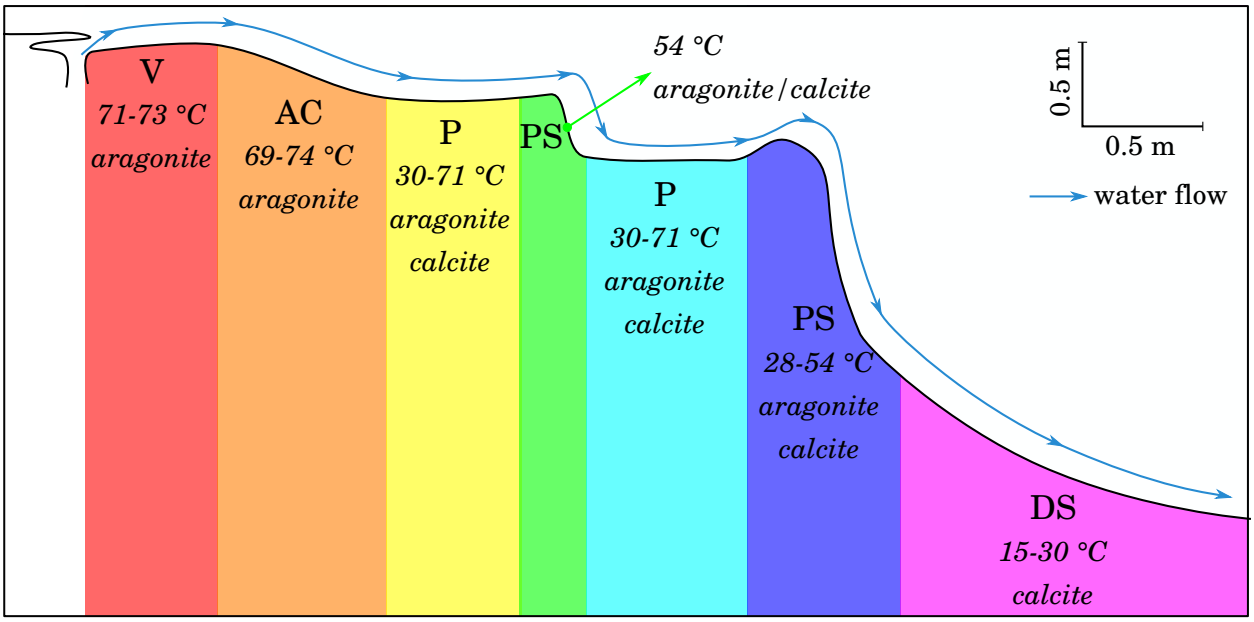

Figure 2.2: Cross section of depositional facies at Angel Terrace, including types of carbonate precipitated and temperature ranges, adapted from *Fouke et al.* [2000] and *Farmer* [2000]. Color loosely correlates with temperature. Key: V = vent; AC = apron/channel; P = pond; PS = proximal slope; DS = distal slope.

2.1.2: Variables

I modified *DLA 3D EXT* to include a spiky starting surface (figure 2.4). These spikes have a user-determined height (H) and spacing (Sp). When particles come within the attraction radius (AR) of the growth surface, they will attach; this process is illustrated in figure 2.5. These are the three variables being explored in this work.

AR

AR handles how close a particle can get before it becomes part of the growth structure. In stromatolite-forming systems, this can correspond to two things: surface charge and stickiness. In systems where surface charge of the growth structure is important, a high AR would correspond to a high surface charge. This comes into play when particles attach to the growth surface through nucleation processes, e.g. in silica-precipitating hot springs.

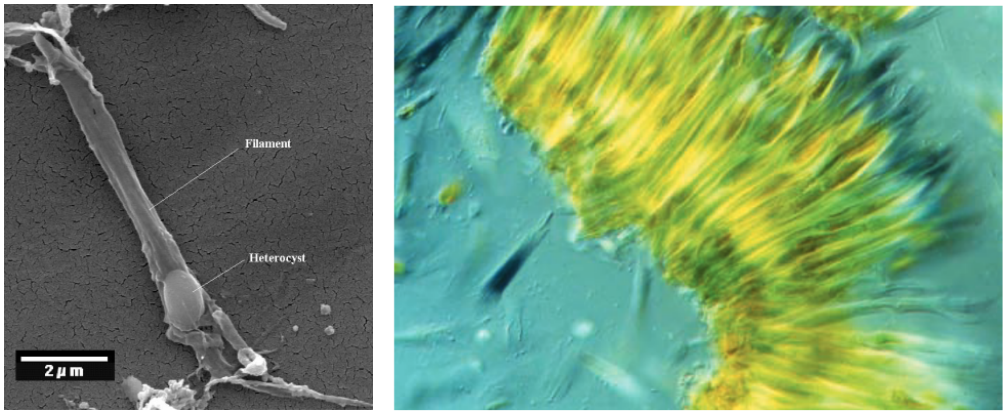

(a) **(b)**

Figure 2.3: (a) Single *Calothrix* cell from *Berrendero et al.* [2008]. (b) *Calothrix* mat from *Norris and Castenholz* [2005]. In (b), the width of most filaments at the base is 4-5μm.

The system modeled in these simulations is a calcite-precipitating hot spring system. In these environments, calcite particles precipitate out of the water, rather than forming through nucleation processes. This means that there are no forces pulling particles in from a distance. Van der Waals forces can cause particles to stick, but these are very short range forces; particles have to touch the surface for van der Walls forces to matter. The only thing causing calcite particles to stick to a surface before they touch is the EPS exuded by microbes.

This means that varying AR is a way to control how "biological" the system is: larger AR can be thought of as more EPS production. At AR = 0, we have an abiotic system where van der Waals forces attach incoming particles.

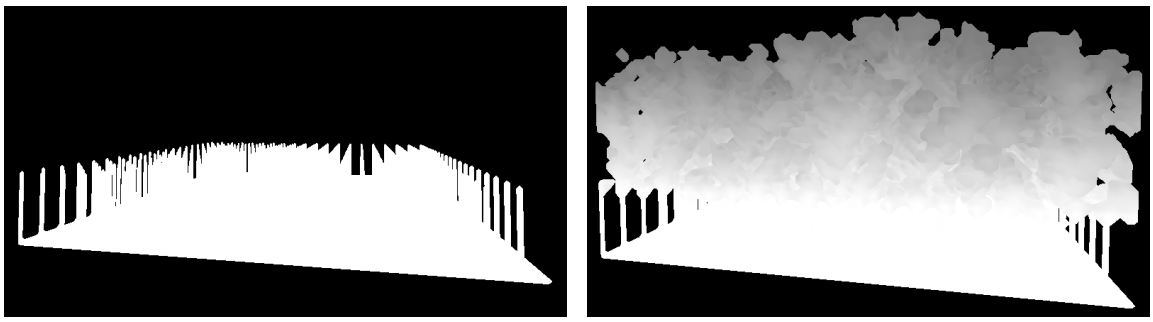

(a) **(b)**

Figure 2.4: Sample spiky starting surface, (a) before and (b) after growth. For this surface, H = 30% of the world height, and Sp = 5 px. Shading added to highlight 3D structure.

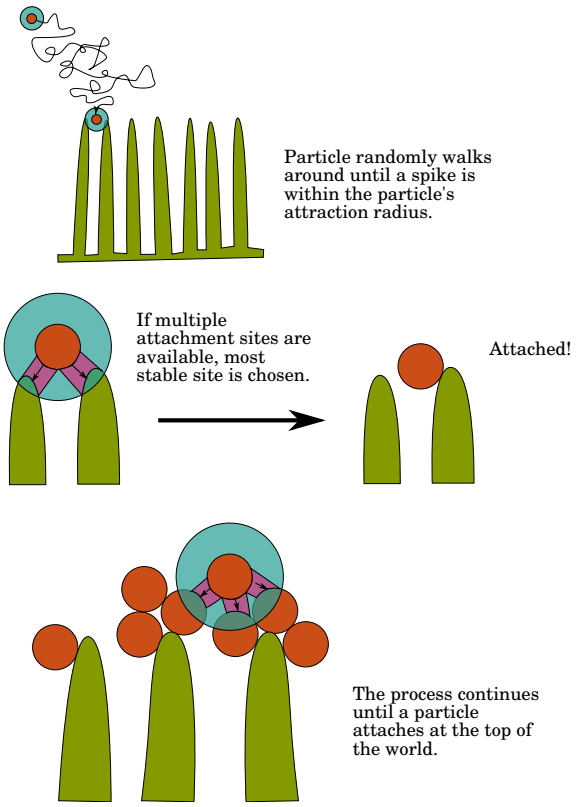

Figure 2.5: Particles attach when they come within a user-defined distance from the growth surface (AR). If multiple potential attachment sites are within the AR, a particle will attach at the most stable site.

Spike Height and Spacing

There are biotic and abiotic spikes in nature. Biotic spikes in a stromatolite-forming system are filamentous microbes, while abiotic spikes may be something like acicular fabrics. Both biotic and abiotic spikes will have some height and some spacing between them. Spikes representing filamentous microbes may vary in height because different species have different heights. They may be more or less spaced out depending on many conditions in a microbial mat: how much EPS the microbes produce, the diversity of microbes in the mat, and the resource requirements for those diverse microbes. Spikes representing acicular fabrics may have varying heights or spacings depending on pressure-temperature conditions at formation.

At Angel Terrace, acicular and shrubby fabrics grow at higher temperatures closer to the vent [*Fouke et al.*, 2000]. So in these simulations that look at the distal slope facies farthest from the vent, spikes can be assumed to be *Calothrix* and therefore biotic. However, a hypothetical abiotic baseline is important to obtain, so AR is still used as a biotic "switch" for all spike heights and spacings.

Calothrix is a morphologically diverse genus and exists in mats with other microbes that have their own range of shapes. These simulations therefore vary spike height and spike

spacing as a way to take that diversity into account. Ranges for all variables were chosen based on what is known about *Calothrix* at Angel Terrace and are explained in detail in section 2.2.2.

2.1.3: Overall Process

Simulations were run to answer these guiding questions:

1. How does changing each of the following affect final stromatolite morphology?
   (a) AR
   (b) Spike height
   (c) Spike spacing
2. How does a change in initial conditions affect stromatolite morphology?
   (a) How is the AR-morphology relationship affected by small/large spike height/spacing?
   (b) How is the spike height-morphology relationship affected by small/large attraction radius/spike spacing?
   (c) How is the spike spacing-morphology relationship affected by small/large sttraction radius/spike height?

Then, for each guiding question, the same process was used:

1. Run simulations in the modified *DLA 3D EXT* Simulator with the appropriate settings.
2. Use the *DLA 3D EXT* Visualizer to capture cross-sections at $\sim 50\%$ through on the XZ plane.
3. Run these cross-section images through fractal analysis software to obtain the fractal dimension (D) and lacunarity (L).
4. Graphically analyze results.

2.2: Coding and Modeling

2.2.1: Modifying *DLA 3D EXT*

A "spike" setting was added to the initial surface options in order to approximate microbial filaments attached to a surface. The relevant code is listed in appendix B.1. Spikes are available on smooth, square starting surfaces or rough, square starting surfaces—that is, the spikes build off the surfaces shown in figures 1.8a and 1.8c. Users can modify spike height and frequency, choosing to have one in the center of the field or several spikes spaced evenly over the field (figure 2.6). Spike height is determined as a fraction of the height of the model world and spacing is determined by a spacing factor (i.e., every nth xy coordinate on the starting surface has a spike on it).

Finally, a small change was made to allow AR to go down to 0 pixels (px); its previous lower limit was 1 px. In abiotic calcite accumulation, particles can attach when they touch the surface, so AR = 0 px represents those conditions.

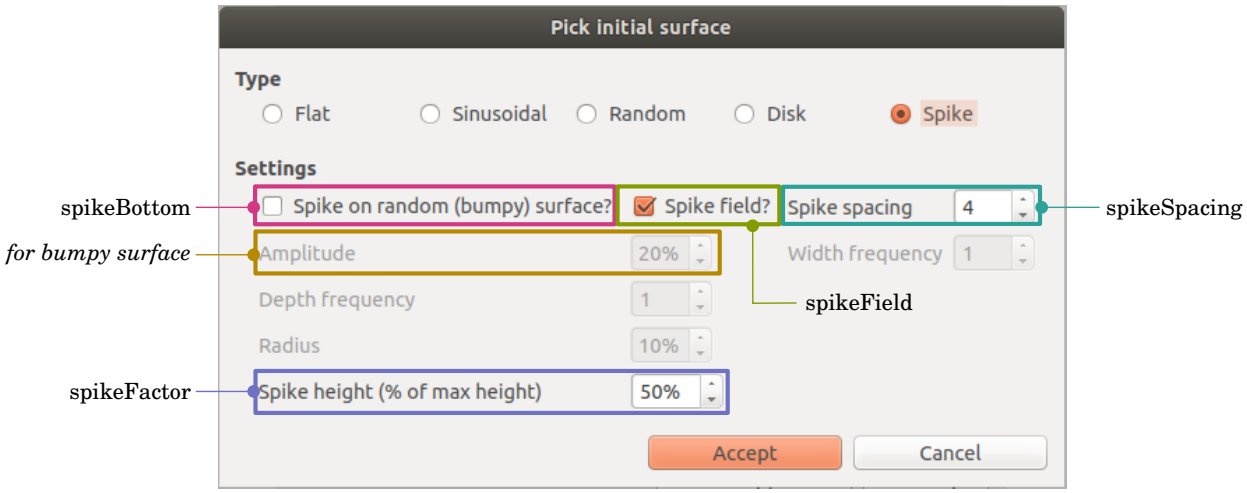

Figure 2.6: Spike settings dialog and corresponding variables in the code. `spikeBottom` and `spikeField` are both booleans; `spikeFactor` describes spike height as a percentage of maximum world height; `spikeSpacing` determines how many pixels apart each spike in a field is placed. These settings will create a field of spikes on an otherwise flat surface. Spikes will be 50% of the maximum world height and placed every 4 pixels along the flat surface.

2.2.2: Simulation

To answer the guiding questions, spike height, spike spacing, and AR were each treated as independent variables. The ranges each covered were:

- $0 \text{ px} \leq AR \leq 5 \text{ px}$

- 10 % $\leq H \leq$ 60%
- 2 px $\leq Sp \leq$ 5 px

Because *Calothrix* filaments in mats tend to be very closely spaced, the range of spacing factors was fairly narrow; based on images of *Calothrix* in mats (e.g. figure 2.3b), Sp = 5 px is likely very extreme. H varied over a larger range in order to take into account the diversity *Calothrix* can have.

Modified *DLA 3D EXT* has available attraction radius (AR) values of integers from 0 px $\leq AR \leq$ 40 px, but it is unrealistic to have an AR any larger than the spike spacing. If AR is a stand-in for EPS, then AR should not be larger than Sp because the EPS will fill the spaces between the microbe filaments. If AR is an abiotic attraction factor, then AR must be zero because the surface charge of calcite is not strong enough to pull in a particle from a distance. So AR was limited to the range $0 \leq AR \leq 5$, since 5 is the largest spacing factor, and likely the absolute largest AR a system like this could conceivably have.

All simulation settings are summarized in table 2.1.

Table 2.1: All simulation settings. Ranges are 0 px $\leq AR \leq$ 5 px; 10 % $\leq H \leq$ 60%; 2 px $\leq Sp \leq$ 5 px. Median values are AR = 2 px, H = 30%, Sp = 3 px.

Question 1: How does changing each variable affect final stromatolite morphology?		
IV	**Held at Median**	**Replicates**
AR	H, Sp	10
AR	n/a (flat surface)	10
H	AR, Sp	10
Sp	H, AR	30

Question 2: How does a change in one variable's initial conditions affect the relationships found in question 1?			
IV	**Set to min/max**	**Held at Median**	**Replicates**
AR	H	Sp	10
AR	Sp	H	10
H	AR	Sp	10
H	Sp	AR	10
Sp	AR	H	10
Sp	H	AR	10

2.3: Image Capture and Analysis

2.3.1: Image Capture and Prep

The *DLA 3D EXT* Visualizer allows users to view, rotate, and take cross-sections of the structures produced by the Simulator. For each simulated stromatolite, a cross-section was taken on the XY plane at either 48% or 50% through, depending on its spacing. If spacing was 2 or 5, the cross section was at 50%; if spacing was at 3 or 4, the cross section was at 48%. This ensured that each cross section went through the spikes. The fact that the cross sections include spikes is not as important as uniformity, but including spikes does allow for analysis of any shapes produced by entombment.

Then, before performing fractal analysis on the resulting images, the images were black/white binarized in ImageJ *Rasband et al.* [1997] so the analysis software would work reliably (figure 2.7). The code used for this is in snippet B.2.

(a) **(b)**

Figure 2.7: Images ready for analysis by FracLac. Settings for (a): AR = 2 px, H = 10%, Sp = 3 px. Settings for (b): AR = 2 px, H = 30%, Sp = 5 px.

2.3.2: Fractal Analysis

Stromatolite cross-sections were run through the FracLac plugin for ImageJ [*Karperien*, 1999–2013; *Rasband et al.*, 1997] to get both their fractal dimension and lacunarity. ImageJ was developed for use primarily for biomedical imaging, where fractal properties can be important diagnostic criteria; for instance, the fractal dimension of packed DNA can be used to identify melanoma cells [*Bedin et al.*, 2010]. FracLac allows ImageJ users to easily determine the fractal dimension and lacunarity of a batch of images, a single image, or region of an image using an implementation of the box-counting algorithm and provides further tools for analysis and interpretation.

For each cross-section, the whole image size (100x50 px) was used as the region of interest. Boxes were no larger than 45px and were allowed to get as small as possible before measured fractal dimension values converged (FracLac calculated this to be 5 px). White was hard-set as the foreground color to ensure the majority color was not treated as foreground. The box counting method can introduce some error depending on box positions, so for a particular box size, the resulting grid was placed over the image in at most 12 different configurations in order to minimize that error. Figure 2.8 summarizes the settings used.

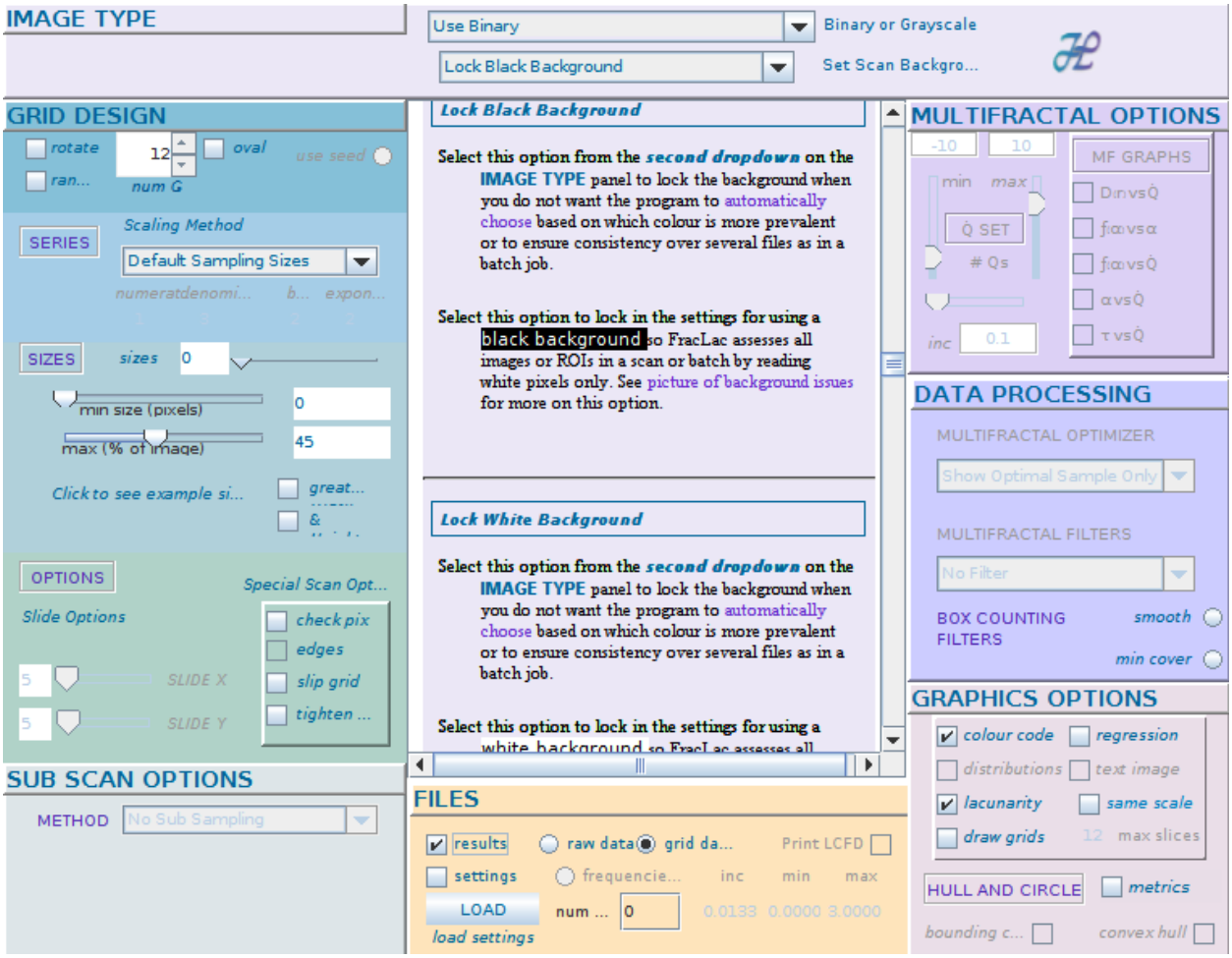

Figure 2.8: The settings I used to obtain my fractal dimension and lacunarity with FracLac.

2.3.3: Data Analysis

FracLac generates a CSV file with all its results; these data were graphed for analysis in R. A warning: many of these graphs look linear and it is tempting to try to fit these to a line and get an equation. However, while the big questions motivating this work are well-studied and, while the methods used to produce and analyze these data are not new, there is very little work exploring the connection between these factors (attraction and filament morphology) and fractal properties. Because of this lack of knowledge, there is no reason to expect that fractal dimension or lacunarity will follow linear trends or indeed fit to any function. Furthermore, it is important to remember that this is all modeled output and in all models, simplifying assumptions are made that may not hold up in the natural systems we are approximating. For instance, in *DLA 3D EXT*, all particles and spikes are one pixel wide, while in a natural system there is a range of both particle and microbe widths. So, in order to avoid overreaching when interpreting the results, the data were not fitted.

Chapter 3: Results and Interpretation

3.1: Question 1: How do attraction radius, spike height, and spike spacing affect final stromatolite morphology?

Table 3.1 describes the simulations run to answer this question and table 3.2 summarizes the results. The following analysis shows that attraction radius has the strongest effect on stromatolite morphology, but introducing a spiky surface appears to reduce that effect.

- Increasing AR clearly decreases fractal dimension and increases lacunarity.
- Increasing spike height has a very small effect on both fractal dimension and lacunarity.
- Increasing spacing slightly decreases fractal dimension, more strongly increases lacunarity.

Table 3.1: Simulation settings for question 1. Ranges are 0 px $\leq AR \leq$ 5 px; 10% $\leq H \leq$ 60%; 2 px $\leq Sp \leq$ 5 px. Median values are AR = 2 px, H = 30%, Sp = 3 px.

Question 1: How does changing each variable affect final stromatolite morphology?		
IV	**Held at Median**	**Replicates**
AR	H, Sp	10
AR	n/a (flat surface)	10
H	AR, Sp	10
Sp	H, AR	30

Table 3.2: The effect of increasing each independent variable on the fractal properties obtained. Key: ↑ = increase, ↓ = decrease, — = flat.

IV	Fractal dimension	Lacunarity
AR ↑	↓	↑
H ↑	—	—
Sp ↑	—	↑

3.1.1: Attraction Radius

There is an inverse relationship between attraction radius and fractal dimension and a direct relationship between AR and lacunarity. These relationships appear to be somewhat better defined for the simulations run on flat surfaces than on spiky surfaces (H = 30%, Sp = 3 px). The flat and spiky sets at each AR do not consistently overlap, suggesting that spike height and AR interact.

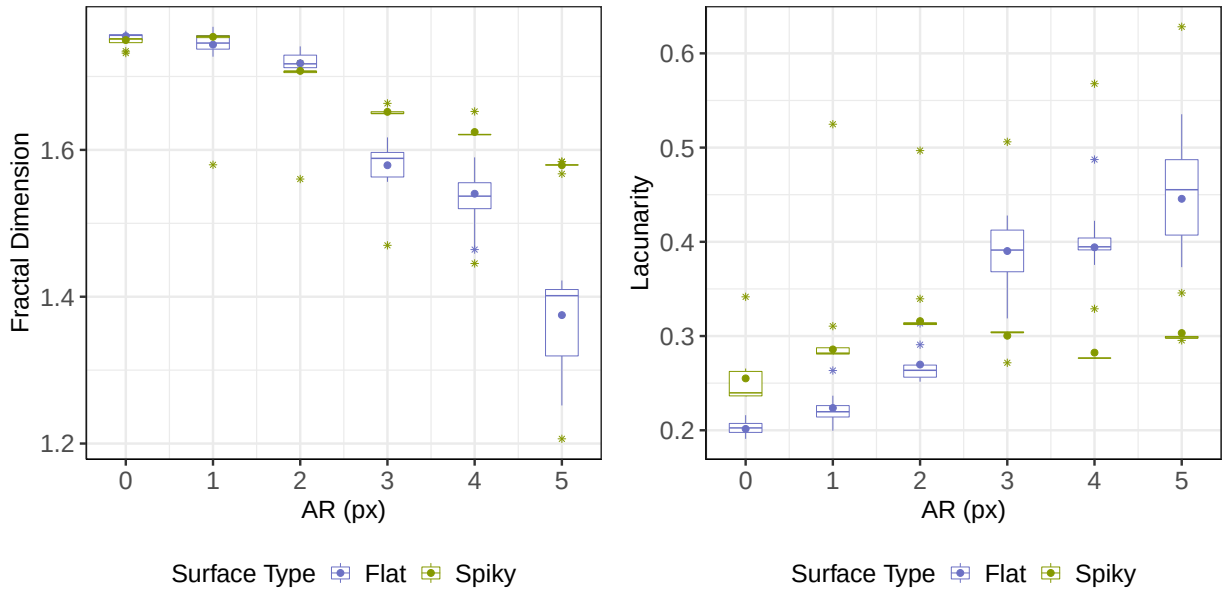

(a) **(b)**

Figure 3.1: Fractal dimension (a) and lacunarity (b) of stromatolites grown on flat (purple) and spiky (green) surfaces as they depend on attraction radius. Asterisks are outliers. Changing attraction radius has an effect on stromatolite morphology. A larger AR will make structures more clustered, with more gaps.

3.1.2: Height

Spike height alone does not appear to affect a stromatolite's fractal dimension or lacunarity. This makes sense based on how the model is constructed. Figure 3.3 shows how particles accumulate on spikes at minimum and maximum height, assuming spacing and AR are held equal. Particle accumulation itself is the same when you look at the space between the top of the spikes and the top of the world (i.e., our simulated water column). The only difference is that the spikes take up more vertical space. The spikes themselves are not complex and, unless we run at the maximum spacing factor and/or minimum AR, it is difficult for particles to get down among those spikes. So there really is no overall change in particle distribution and clustering.

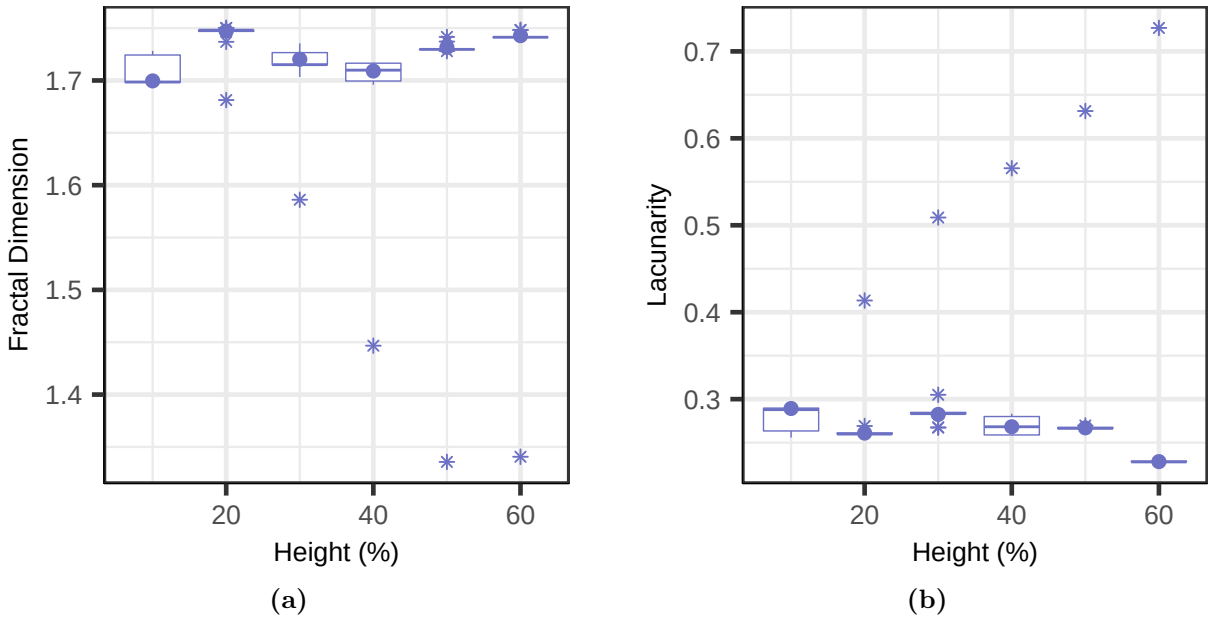

Figure 3.2: Fractal dimension (a) and lacunarity (b) of modeled stromatolites as they depend on spike height.Changing spike height has no effect on stromatolite morphology. The outliers appear to form a line. These all came from the earliest batch of simulations and is likely due to user error in setting up FracLac analysis.

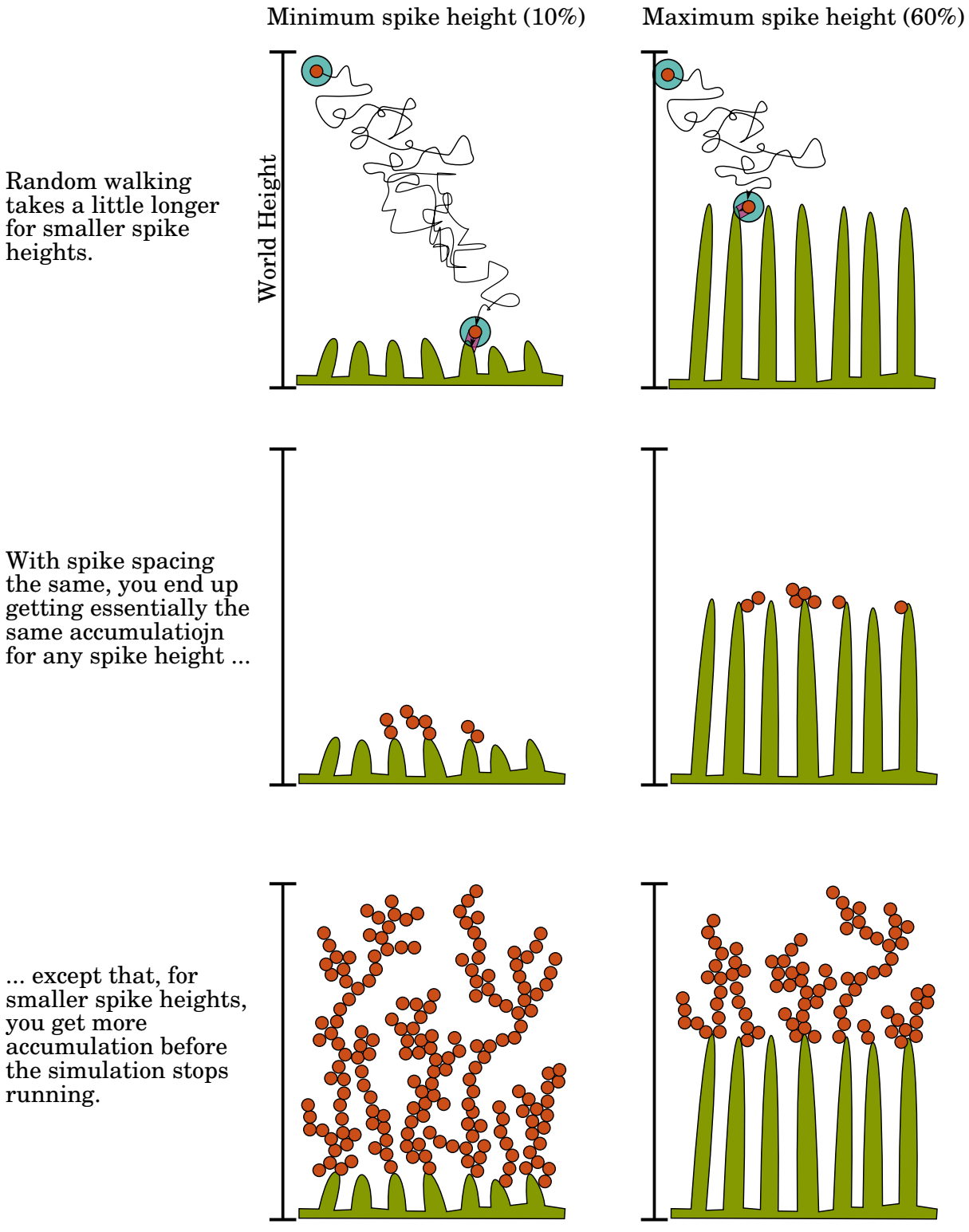

Figure 3.3: The effect of height on particle accumulation.

3.1.3: Spacing

Spacing does not appear to strongly affect a structure's fractal dimension, as the boxplots do not appear to have a clear organization. However, spacing *does* affect lacunarity: increasing space between spikes causes an increase in lacunarity.

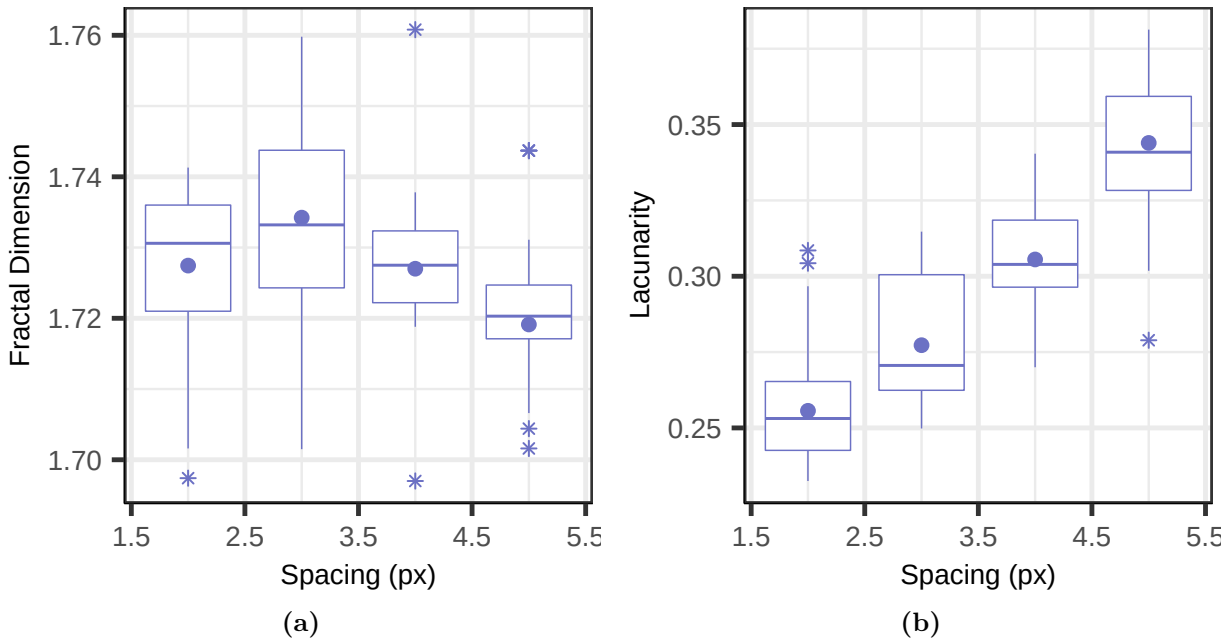

Figure 3.4: Fractal dimension (a) and lacunarity (b) of modeled stromatolites as they depend on spacing factor. Changing spacing has an effect on stromatolite morphology, but only as measured by lacunarity.

It seems on its face that this should make sense—because lacunarity measures gappiness, and gaps are just space, then increasing the space should increase the lacunarity.

However, increasing the spacing factor actually increases the *available* space for particles to come in to occupy, so it would make sense to expect less gappiness in the high-spacing simulations. But this does not appear to be the case—at least, not at the current attraction radius of 2. Figure 3.5 illustrates how particles with AR = 1 accumulate on spikes with either minimum or maximum spacing. Because the filaments and the particles have the same diameter, rather than very small particles relative to filament size, the few particles that can make it down among the filaments quickly block off that route for the rest of the particles. If *DLA 3D EXT* supported manipulating particle size, we could test to see if the opposite relationship occurred with very small particles.

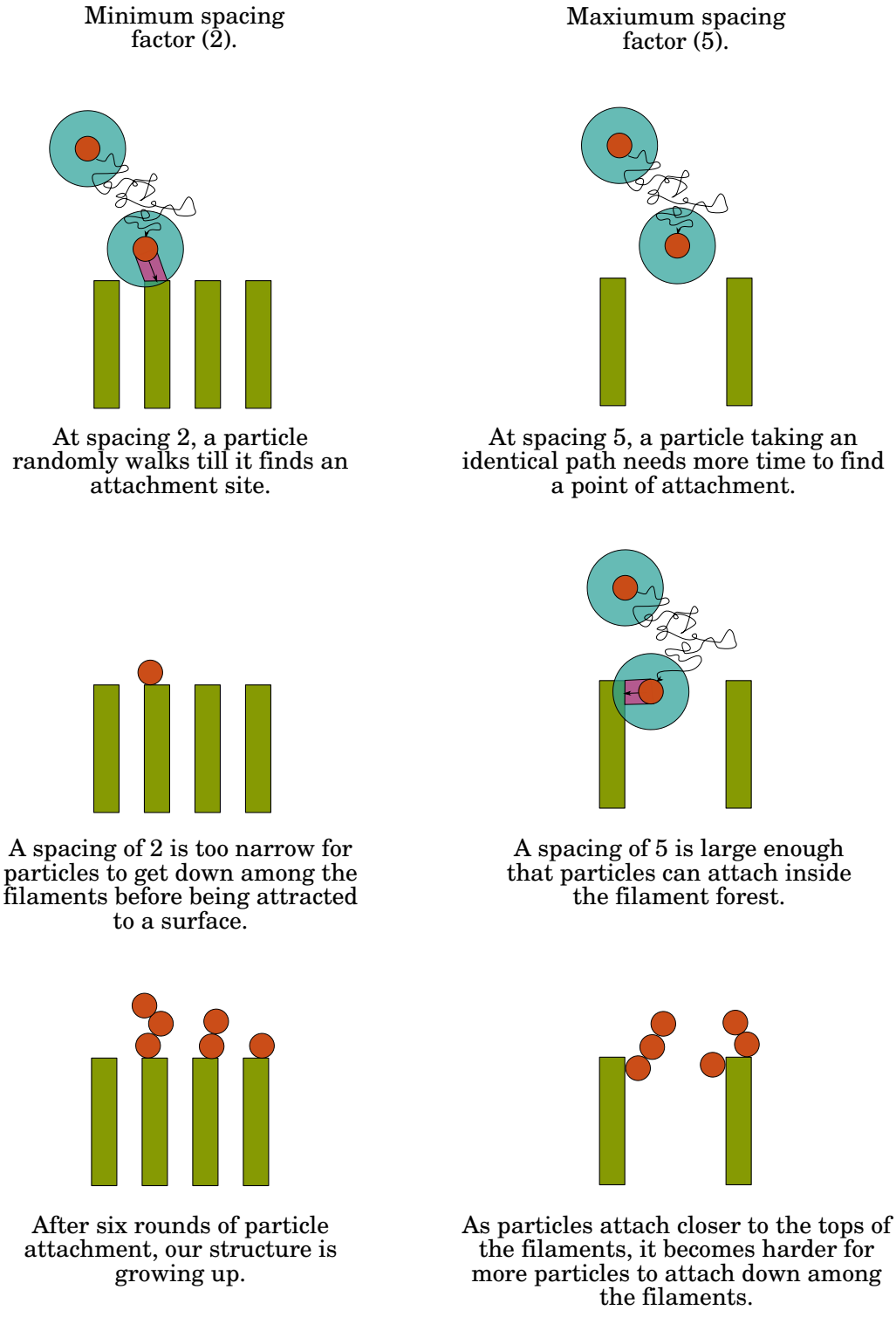

Figure 3.5: The effect of spacing on particle accumulation.

3.2: Question 2: How does a change in initial conditions affect stromatolite morphology?

The additional simulations run to answer this question (table 3.3) were integrated with the data from section 3.1. This allowed for easy comparison with those initial data and to see a progression from changing a parameter's initial conditions from minimum to median to maximum.

The following analysis shows that AR and spike height interact with each other, but changing any parameter while changing spacing initial conditions yields messy results. Further, the conclusion from section 3.1 that spacing affects lacunarity is contradicted here: spacing does not affect lacunarity; the AR settings used for those simulations produced those results.

To summarize the results (table 3.4 offers further summary):

- How is the AR-morphology relationship affected by changing height and spacing initial conditions?
  - Changing height initial conditions produces larger differences in both fractal dimension and lacunarity at higher AR. (See section 3.2.1 for more detail.)
  - Changing spacing initial conditions does not affect how fractal dimension trends with AR and makes the relationship between AR and lacunarity unpredictable. (See section 3.2.1 for more detail.)
- How is the height-morphology relationship affected by changing AR and spacing initial conditions?
  - Changing AR initial conditions when exploring spike height reinforces the spike height/AR relationship shown when exploring AR and changing spike height conditions. (See section 3.2.2 for more detail.)
  - Changing spacing initial conditions does not appear to affect the relationship between spike height and morphology. (See section 3.2.2 for more detail.)
- How is the spacing-morphology relationship affected by changing AR and height initial conditions?
  - Changing AR initial conditions gives lower fractal dimension across the range of spacing, but spacing does not affect the fractal dimension for any specific AR. (See section 3.2.3 for more detail.)
  - Changing spike height initial conditions does not affect the relationship between spacing and morphology. (See section 3.2.3 for more detail.)
  - When AR = 2 px, lacunarity appears to follow an upward linear trend, but this

is due to the AR-morphology relationship.

Table 3.3: Additional simulations for question 2. Ranges are 0 px $\leq AR \leq$ 5 px; 10% $\leq H \leq$ 60%; 2 px $\leq Sp \leq$ 5 px. Median values are AR = 2 px, H = 30%, Sp = 3 px.

Question 2: How does a change in one variable's initial conditions affect the relationships found in question 1?			
IV	**Set to min/max**	**Held at Median**	**Replicates**
AR	H	Sp	10
AR	Sp	H	10
H	AR	Sp	10
H	Sp	AR	10
Sp	AR	H	10
Sp	H	AR	10

Table 3.4: The effect of changing initial conditions on the relationships in table 3.2. Key: ↑ = increase, ↓ = decrease, — = flat.

IV	IC change	Fractal dimension	Lacunarity
AR ↑	None (from table 3.2)	↓	↑
	H min	↓ at lower rate	↑ at lower rate
	H max	↓ at much lower rate	↑ at much lower rate
	Sp min	no effect	no effect
	Sp max	no effect	difficult to interpret
H ↑	None (from table 3.2)	—	—
	AR min	no effect	no effect
	AR max	↑	↓
	Sp min	no effect	difficult to interpret
	Sp max	no effect	difficult to interpret
Sp ↑	None (from table 3.2)	—	↑
	AR min	no effect	—
	AR max	no effect	—
	H min	no effect	no effect
	H max	no effect	no effect

3.2.1: How is the AR-morphology relationship affected by changing height and spacing initial conditions?

Changing height initial conditions

For these simulations, it is possible to integrate the data from the previous AR simulations (i.e., from figure 3.1) to look at a larger range of spike height/AR pairs, shown in figure 3.6.

For both fractal dimension and lacunarity, the values seem to be similar at low AR for all spike height subsets; however, progressing to high AR shows a separation and sorting of spike height subsets. At AR = 5, simulations run with the two extreme spike heights of 0% and 60% have the most extreme fractal properties, and the simulations run at 10% and 30% settle in ascending order. That is not true at all AR, however: the lacunarity values at 0 px $\leq$ AR $\leq$ 2 px, for instance, show no correlation between spike height and lacunarity.

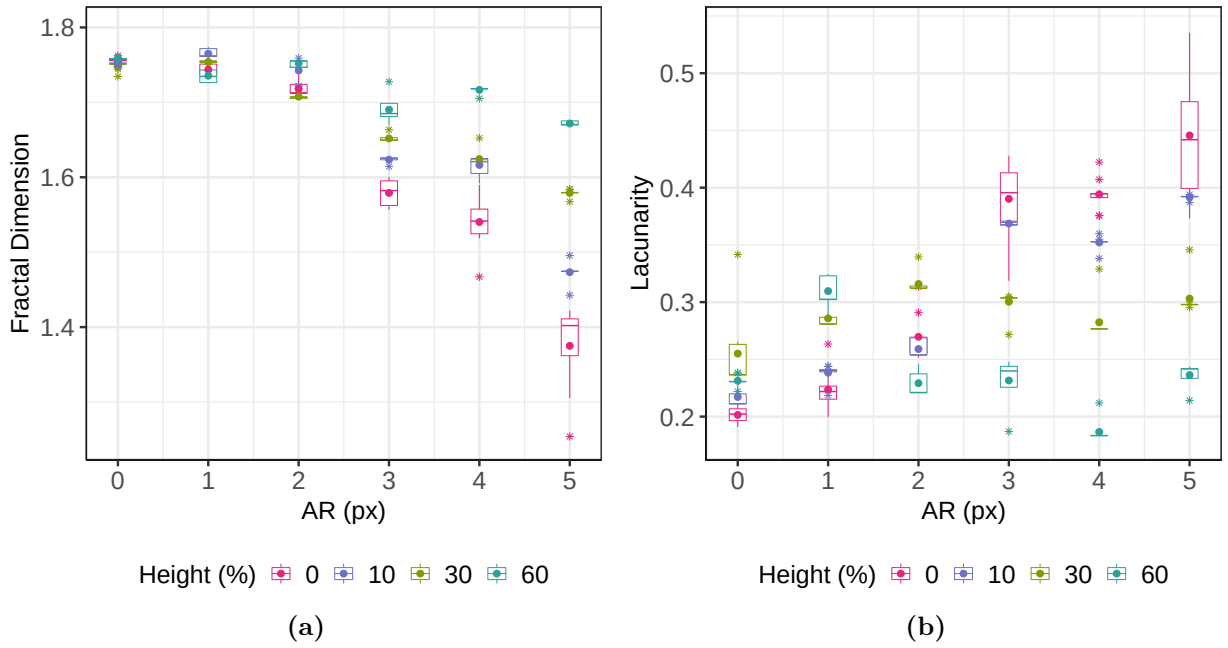

(a) **(b)**

Figure 3.6: Fractal dimension (a) and lacunarity (b) of modeled stromatolites as they depend on attraction radius. The AR-morphology relationship is affected by changing height initial conditions. A larger height dampens the AR-morphology relationship.

Changing spacing initial conditions

Changing spacing does not appreciably affect the relationship between AR and fractal dimension. Figure 3.7a shows that the Sp = 2 px, Sp = 3 px (from figure 3.1) and Sp = 5 px boxes overlap, indicating that changing spacing factor doesn't affect the downward trend in fractal dimension from low to high AR.

However, spacing *does* affect the relationship between AR and lacunarity (figure 3.7b): there are clear diffrences between the Sp = 2 px, Sp = 3 px, and Sp = 5 px groups. Moving from low to high spacing, the relationships between AR, spacing, and lacunarity seem to be getting less well defined.

As figure 3.5 demonstrates, a small AR and a high spacing should produce structures with lower lacunarity; that is, there is more room for particles to get down among the filaments due to high spacing and particles can get into tighter spaces due to lower AR. But the data here do not support that prediction, especially at the AR = 1 px, Sp = 5 px box. The reason for this is unclear and warrants further study.

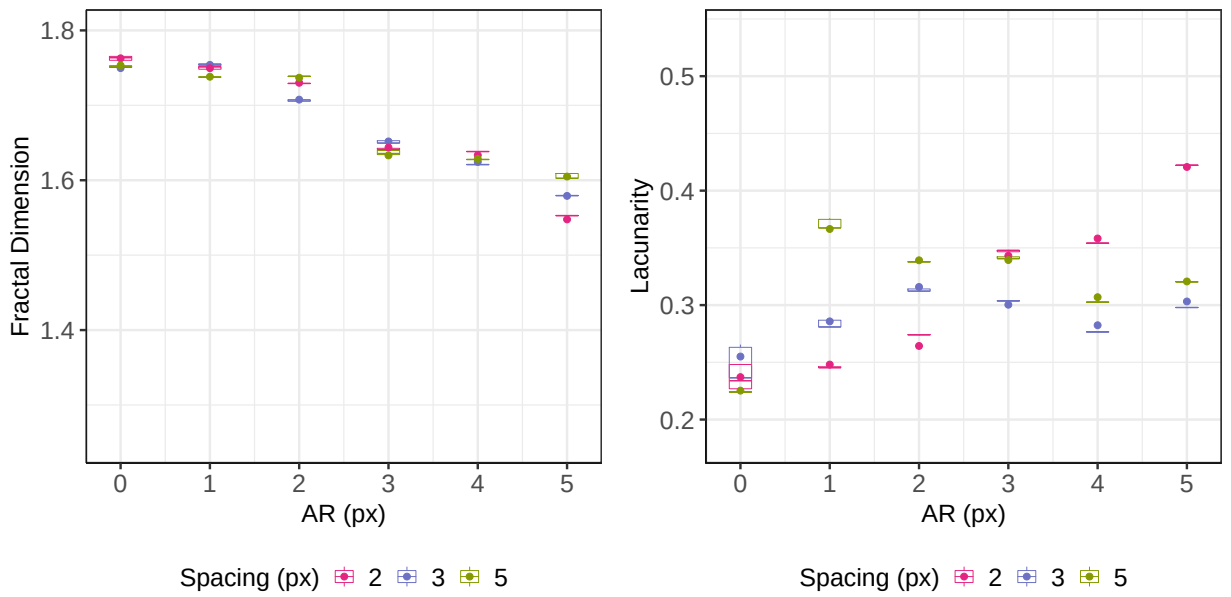

Figure 3.7: Fractal dimension (a) and lacunarity (b) of modeled stromatolites as they depend on attraction radius. The AR-fractal dimension relationship is not affected by chanigng spacing initial conditions, but the AR-lacunarity relationship is, in a way that is difficult to interpret.

3.2.2: How is the height-morphology relationship affected by changing AR and spacing initial conditions?

Changing AR initial conditions

These data provide further support for the interpretation in section 3.2.1. In figure 3.6, the data at AR = 0 px and AR = 2 px are somewhat clustered together with little to no separation by spike height, suggesting that spike height does not impact the structure much at low AR. Similarly, in figure C.1, fractal dimension and lacunarity are fairly consistent across all spike heights when AR = 0 px and AR = 2 px, and the AR = 2 px data are consistently lower than the AR = 0 px data. So figure C.1 shows the same sorting from figure 3.6.

This is further supported by the AR = 5 data in both simulation sets. In figure C.1, the upward trend shows that increasing spike height by 10% has a large effect on both fractal dimension and lacunarity. And in figure 3.6, we see that difference as sorting by spike height at AR = 5.

Changing spacing initial conditions

Changing spacing initial conditions did not yield any discernable patterns in the height-morphology relationship (figure 3.8). It is possible to describe each spacing subset at each height value relative to each other and it is possible to describe each spacing subset's behavior over the range of heights, but it is difficult to pull out a general trend or rule to describe how spacing initial conditions affect the spike height-morphology relationship. There does not seem to be any sorting by spacing or flattening by spacing: changing spacing initial conditions has an unpredictable effect on morphology.

This is also true for the AR-morphology relationship, at least for lacunarity. Figure 3.7b is similarly difficult to interpret. Spacing appears to be a complicating factor and one that warrants more investigation.

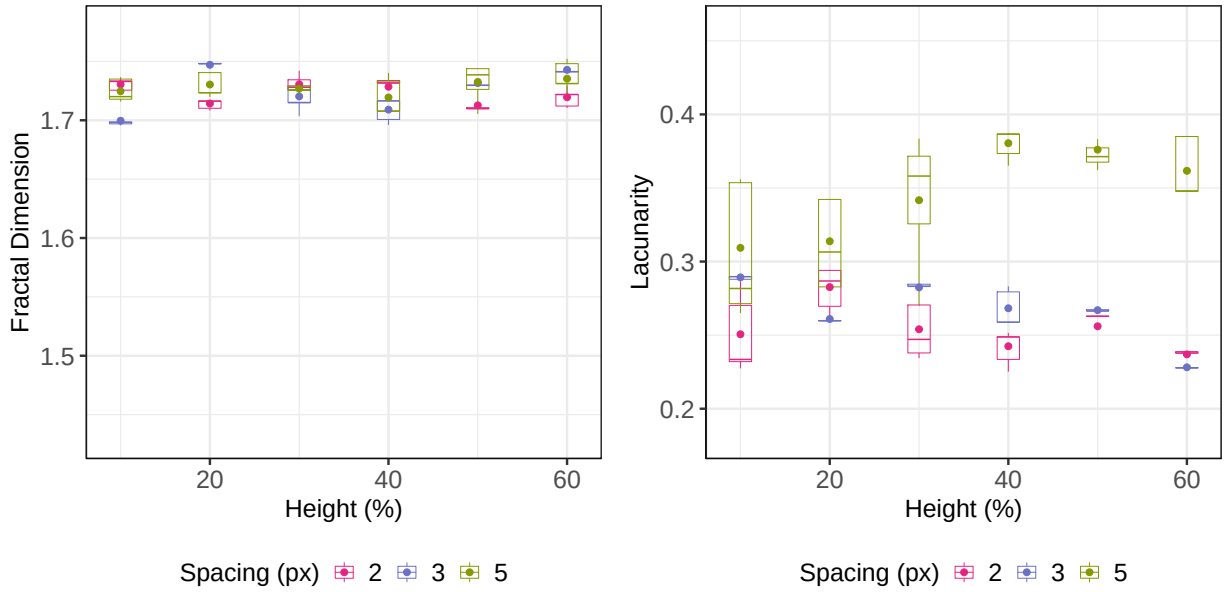

(a) **(b)**

Figure 3.8: Fractal dimension (a) and lacunarity (b) of modeled stromatolites as a function of spike height. The height-lacunarity relationship is affected by changing spacing initial conditions; however, there does not seem to be any pattern produced by those changes.

3.2.3: How is the spacing-morphology relationship affected by changing AR and height initial conditions?

Changing AR initial conditions

Spacing does not appear to affect fractal dimension, but AR does: all AR groups are essentially flat as spacing increases, but lower AR groups have higher fractal dimension (figure 3.9a). This supports the previous interpretations that AR has a strong effect on fractal dimension.

Lacunarity is a little more difficult to interpret (figure 3.9b). Increasing spacing may increase lacunarity at AR = 2 px, but this relationship doesn't hold true when AR = 0 px or AR = 5. Indeed, AR = 2 px might be an attraction radius that starts preventing particles from falling down among the filaments. To verify this, figure 3.10 shows a sample cross section from each spacing/AR combination. At AR = 0 px, particles can fall in between the spikes; by AR = 2 px, they can't. There is a clear separation between filaments and accumulation: there are no particles below that line. If the lacunarity of the filament region grows while the lacunarity of the accumulation region stays the same, this could explain that upward trend for the AR = 2 px data in figure 3.9b. The lacunarity of the accumulation region may vary enough to produce no clear trend at AR = 5. These data have larger boxes, and therefore

larger spread, than the AR = 2 px data.

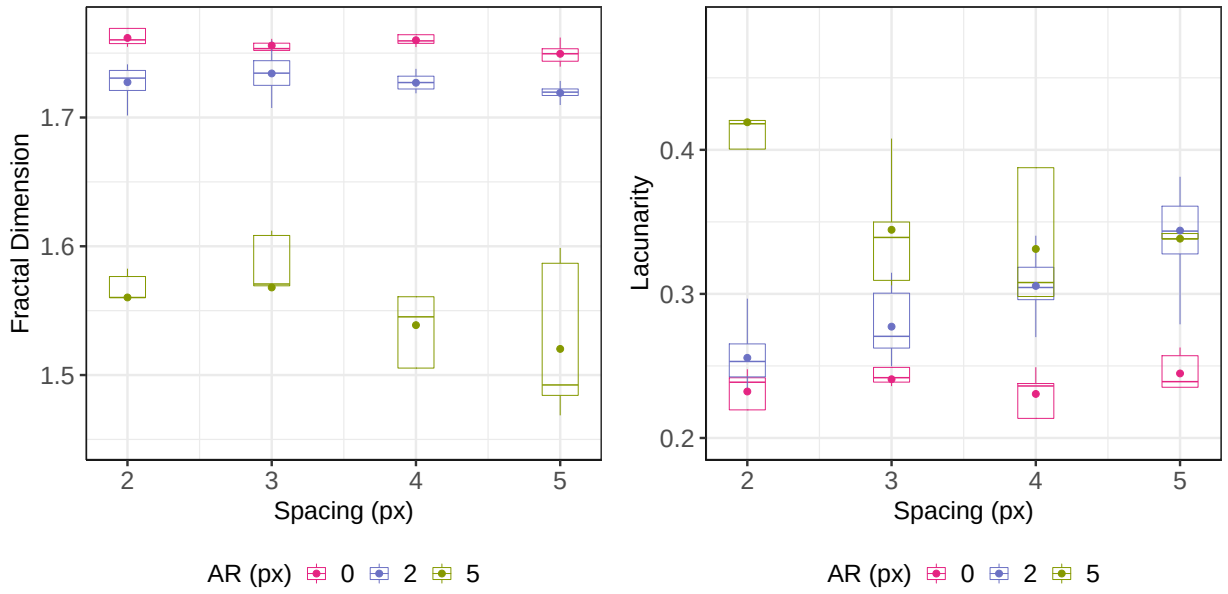

(a) **(b)**

Figure 3.9: Fractal dimension (a) and lacunarity (b) of modeled stromatolites as a function of spacing. The spacing-morphology relationship is not affected by changing AR initial conditions. The apparent relationship between spacing and lacunarity at AR = 2 px is an artifact.

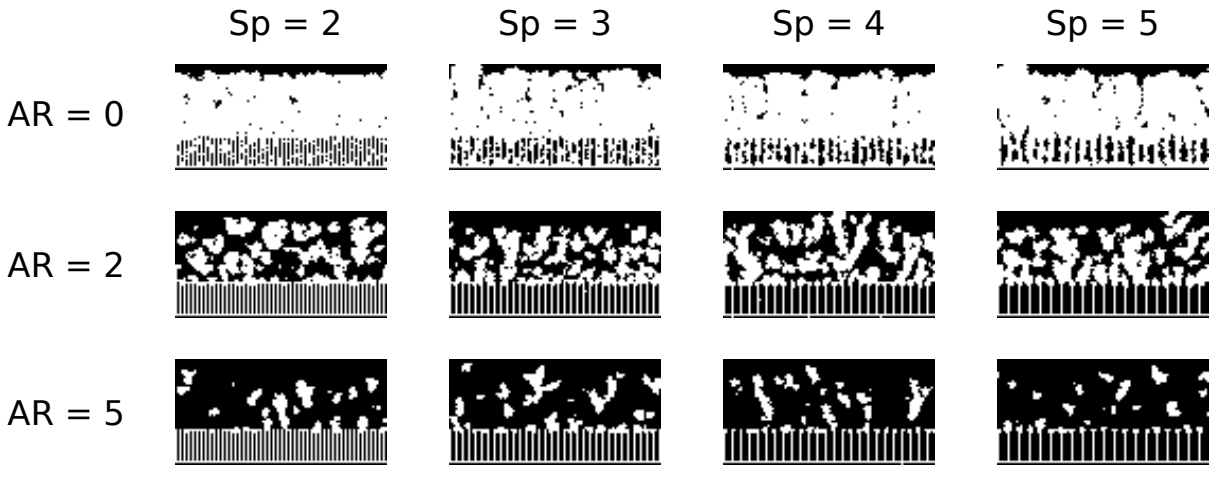

Figure 3.10: Sample cross sections from each spacing/AR combination used in this analysis.

Changing height initial conditions

There is no clear relationship between spacing and morphology when changing height initial conditions (figure C.2). No clear pattern emerges in fractal dimension as height initial conditions are changed, but each height subset looks relatively flat. For lacunarity, the spike height subsets appear to follow an upward trend together with enough overlap that it looks like height initial conditions have no effect on the spacing-lacunarity relationship. The relationship appears to be a consequence of keeping AR = 2 px for all simulations.

Chapter 4: Discussion and Conclusion

4.1: Appyling these results to the natural system

Attraction radius appears to be the most important factor in determining a stromatolite's morphology. A higher attraction radius consistently yields a lower fractal dimension and a higher lacunarity, regardless of initial conditions. This means that a higher AR creates a more clustering of particles and larger gaps in the structure.

In the travertine hot spring system approximated by this model, AR corresponds to EPS production. The model assumes that calcite particles precipitate out of the water to fall on our structure rather than adhering to the structure through nucleation processes, which means that electrostatic or point of zero charge factors are negligible. For particles sticking to a surface without those factors, the only possible attractive force is the van der Waals force, which falls off quickly with distance: van der Waals forces are essentially what is represented by AR = 0 px. We can consider any higher AR value to be EPS. So in a calcite system, a more clustered structure (i.e., one with lower fractal dimension) is likely to be biogenic. Based on the values obtained from these simulations, a fractal dimension less than 1.6 suggests high EPS production.

It may be possible to connect the clustering in a stromatolite with the conditions that affect EPS production. EPS production is in part a way for microbes to protect themselves from entombment by incoming particles. Of course, it is circular to say that particles were falling on a microbial mat because a stromatolite has high clustering: that is how stromatolites form. But it may say something about the rate of particle accumulation.

EPS is also a medium for cell-to-cell communication, coordinating the growth and integrity of the mat. The amount of EPS production therefore may also be connected to the number and types of microbes in the mat. More research into how EPS production varies by community diversity would be needed to make more inferences about stromatolite-forming communities.

Spike height affects the strength of the AR-fractal dimension relationship: a higher spike height dampens the effect of AR on clustering (see figure 3.6). This may have significant applications or it may be a consequence of the limits of the model.

Spike height can be interpreted as microbe filament height. Going with that interpretation presents a problem with the model: microbes are flexible and soft-bodied, while the spikes in the model are not. Microbes deforming as a calcite layer accumulates is not something the model can handle and that would certainly affect how particles might fall between microbes. Furthermore, while the spikes in the model remain even when they are not completely entombed, this is not true for microbes. Microbes die and decompose and are no longer a part of the stromatolite structure. As figures 3.3 and 4.1 demonstrate, accumulation above

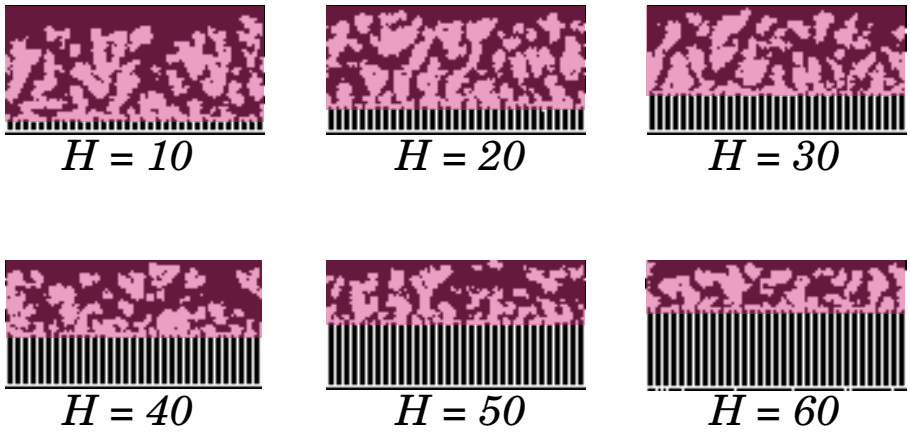

Figure 4.1: Accumulation above the spikes (pink) is unaffected by the spikes below; only the pink regions will be preserved if the filaments below decompose.

the spikes is unaffected by the spikes. So, if microbes disappear, all that is left is the upper accumulation that was unaffected by the spikes, regardless of their height.

Spike height can also be interpreted as the height of abiotic spikes. In travertine springs, acicular fabrics can form [*Fouke et al.*, 2000]. But abiogenic environments have very low AR, and at low AR, varying spike height produces almost no effect. Particles are able to pack in too tightly for spike height to appreciably alter the fractal dimension or lacunarity because they essentially subsume the spikes into the broader structure.

So while the model shows that spike height and AR interact, especially when both are larger, those results do not apply well to actual stromatolites.

While the spike spacing results were difficult to interpret, it may not matter in application. In a natural setting, a larger spike spacing may only apply to abiotic spikes, as *Calothrix* and other mat-forming microbes tend to pack very closely. So investigating spike spacing could potentially have borne some interesting fruit: if there were a clear relationship between spike spacing and stromatolite morphology, it could be exploited to better distinguish true stromatolites from abiotic impostors. But based on the results of the simulation, this line of investigation appears to be a dead end: spike spacing does not affect stromatolite morphology much at all.

So in the end, the only relationship that appears to help discern calcite stromatolites from other layered rock structures is the AR-morphology relationship.

This suggests that the practice of assigning genus names to stromatolites is inappropriate, at least for carbonate stromatolites. AR corresponds to EPS production and the amount of EPS produced in a microbial mat is not exclusively species-dependent. EPS production depends not only on microbial activity, but also on the rate of entombment and other external stressors to the microbial community. So if EPS is the dominant factor in stromatolite morphology, stromatolites may not preserve enough information about the communities that formed them

for any real taxonomy to be done.

At this point, it is important to address two questions about the methods used.

1. Are the fractal dimension numbers applicable to natural stromatolites?

2. Are the lacunarity numbers applicable to natural stromatolites?

Because this model still needs to be ground-truthed, it is impossible to give definite answers to these questions. However, some predictions can be made.

If the fractal dimension results are applicable, lab and field work may reveal one of two things. The fractal dimension values obtained here may perfectly predict what occurs in nature. If so, true stromatolites should have fractal dimensions lower than 1.6, while abiotic layered structures should have fractal dimensions higher than 1.7. Another possibility is that the values may change, but the pattern may not; that is, true stromatolites may have consistently lower fractal dimension than abiotic layered structures, but the threshold values of 1.6 and 1.7 may be different. Testing these predictions would require controlled lab work to quantify microbes' EPS production, culture organisms that produce increasingly large amounts of EPS, and let calcite precipitate out onto the mats. If this model does reflect the natural world, such experiments should show a decreasing fractal dimension with increasing EPS production. Section 4.2.1 describes potential future work in more detail.

If the lacunarity results are applicable, then the same lab work confirming the fractal dimension results should confirm the lacunarity values. However, there is a geometric argument against using lacunarity in a 2D application as it was used here.

A good way to conceptualize the problem is to think of a block of Swiss cheese. The cheese is all connected in one structure, but the holes inside are not. After the block of cheese is sliced, different slices will have different gap distributions, making it impossible to characterize the whole block of cheese from the gap distributions of any randomly chosen slice. Therefore, to use lacunarity to characterize the whole block of cheese (or the layered rock structure), the entire volume needs to be considered.

It is technically possible to do this with the model and image analysis methods as they exist now. Rather than taking one cross section from each stromatolite and using it to represent the whole, a cross section from each potential slice point could be taken and all those cross sections could be analyzed. FracLac can handle 3D stacks of images or a distribution of lacunarities could be built from each cross section. However, taking all those slices is currently such a time- and labor-intensive process as to make it impracticable. Section 4.2.2 discusses ways to address this issue.

4.2: Future Work

4.2.1: Model and Result Validation

For Calcite Stromatolites

Field work and lab work can both verify the applicability of these results and the scientific accuracy of the model. While samples of biofabrics have been taken at many travertine springs, including at Mammoth [*Fouke*, 2011], they have not been analyzed using the methods here. Carrying out fractal analysis on samples from Mammoth Hot Springs would provide the beginnings of a ground truth for this work. Extending those studies to other travertine springs could provide some robust evidence for whether this model is accurate.

Lab work would also be a controlled way to validate this model. *Calothrix* mats can be grown in a lab setting (e.g. *Benning et al.* [2004]; *Yee et al.* [2003]), so growing *Calothrix* in an aquarium set up to mimic the conditions at Mammoth could allow for a controlled replication of travertine stromatolites. Further, a microbial mat's EPS yield can be measured using the procedures developed by *Klock et al.* [2007].

It is possible, then, to verify the results presented here in the lab. Cultivating mats with differing net EPS yields in a simulated-Mammoth aquarium would produce lab-grown stromatolites to be analyzed. Comparing the fractal dimensions of sections from the lab stromatolites to these results would be a first step to verifying whether AR is a good analogue for EPS. If it is, then further experiments in this vein could allow AR values to be directly matched to EPS yield.

Extending to Other Stromatolites

Not all stromatolites form through trapping and binding. Silica stromatolites form through nucleation of particles directly onto the growth surface [*Hugo et al.*, 2011]. For such systems, high AR is no longer an indicator of biogenicity; instead, it may represent abiotic factors such as surface charge. This model shows what structures form from high AR; an interesting project would be to manipulate a silica-precipitating system to try to replicate those structures.

4.2.2: Model Improvement

It is impossible to perfectly replicate a natural system, so when building a model, it is necessary to make approximations and simplifications. For instance, the spikes added to this model are not flexible like microbial filaments are, which affects the structures produced by the software. But, given the time and programming ability available, it is beyond the scope

of this project.

Similarly, the movement algorithm as written by *Chappatte* [2010], while billed as Brownian, is not truly. Algorithm 2 shows how particles move. Whether a particle moves on an axis is determined randomly or semi-randomly, so it is a random walk; however, the possible velocities are fixed. For each direction, a particle can move one pixel per time step or not at all.

Algorithm 2: Actual particle movement in *DLA 3D EXT*.

```
Data: zValue, x, y, z
Result: new particle position
for calcite particle do
    double d = random(0, 1);
    if d < zValue then # zValue favors downward movement
        z–;
    end
    else
        if d >= zValue then
            z++;
        end
    end
    if z above or below world then
        Start a new particle;
        Return;
    end
    d = random(0, 1);
    if d < 1.0 / 3.0 then
        x++;
    end
    else
        if d >= 2.0 / 3.0 then
            x–;
        end
    end
    d = random(0, 1);
    if d < 1.0 / 3.0 then
        y++;
    end
    else
        if d >= 2.0 / 3.0 then
            y–;
        end
    end
end
```

This is not physically accurate. Movement from collisions with surrounding particles results in a distribution of potential velocities, because the surrounding particles themselves have a range of velocities. In gases, this is the Maxwell-Boltzmann distribution, but liquids follow something similar. It depends on the masses of the particles involved, the average temperature of the system, and the fluid properties of the diffusion medium.

Chappatte used an approximation that allowed him to write a general function for particle movement, rather than the many functions that would be needed to take into account particle masses, temperature, and fluid dynamics. But approximations may still give suitable results. A way to test whether this approximation works would be to track the movement of a particle following this algorithm and compare that to the movement of a particle in Brownian motion.

In one-dimensional Brownian motion, a particle's root mean square displacement, $\sqrt{\bar{x}^2}$, is

$$\sqrt{\bar{x}^2} = 2D_d\sqrt{(t)}, \tag{4.1}$$

where D_d is the diffusion coefficient, determined by the properties of the particle and the diffusion medium, and t is time [*Klafter et al.*, 1996]. This means that $\bar{x}^2$ is proportional to t.

If Chappatte's algorithm is a good approximation, then tracking one dimension of a particle's movement over many iterations and graphing $\bar{x}^2$ against t should produce something like a straight line. Snippet B.3 contains the code used to do that and figure 4.2 is the resulting graph. The movement in z (figure 4.2b) looks exponential rather than linear, while

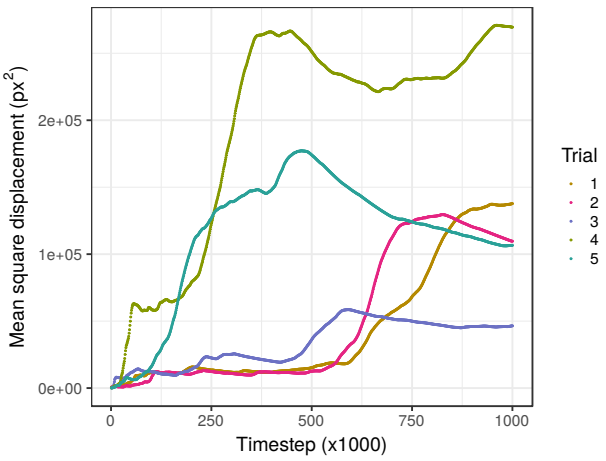

(a) A particle's mean square displacement vs. time for 1D movement in the z direction.

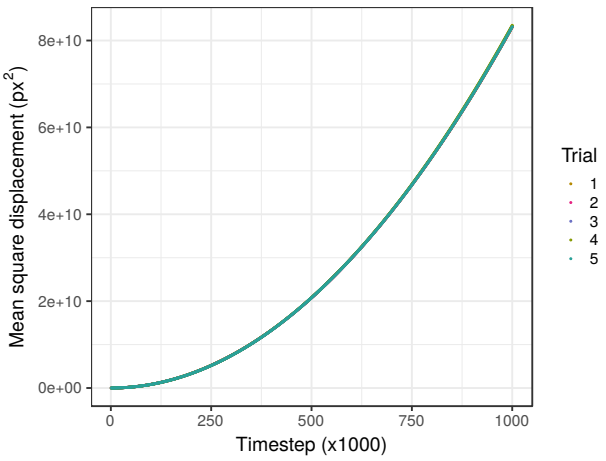

(b) A particle's mean square position vs time for 1D movement in the x direction. Particles undergo the same type of movement in y.

Figure 4.2: Graphs of the motion produced by algorithm 2. Brownian motion would produce a straight line.

the movement in x and y (figure 4.2a) shows no trend. This suggests that Chappatte's approximation is flawed and this may affect the structures produced by the model. Modifying the algorithm to more accurately reflect Brownian motion and comparing the resulting structures with those used in this thesis could more definitively answer that question.

There are some further aspects of the model that could be improved with some thoughtful programming. Everything is one pixel wide, meaning particles are as wide as the spikes and that there is no range of particle sizes or spike widths. Considering that this model and this analysis is entirely about shape, having a wider range of particle shapes and sizes could certainly affect the model output. A more interesting, accurate model would allow for width resizing and potentially a range of widths in a single simulation. Similarly, spike height is currently uniform, but microbial mats are made of morphologically diverse organisms. Allowing for multiple spike heights on a single starting surface, maybe drawn from a random distribution with user-inputted mean and standard deviation, could make a starting surface that is more realistic.

Finally, the number of simulations run was limited by how many images that could be realistically captured and processed by hand. Automating that process would let users run and analyze substantially more simulations, with less room for user error. This would require substantial editing of the Visualizer component of *DLA 3D EXT* to allow a user to set up a batch sectioning process. Ideally, a user would be able to direct the Visualizer to a folder of simulation files and choose how many sections to be taken from each image and where in the image those sections should be taken. Such an improvement would greatly expand the type of image analysis that can be done on these simulations, make future work much easier, and make results more reliable.

References

Amand, A. S., R. B. Hoover, G. A. Jerman, J. Coston, and A. Y. Rozanov (2005), Morphology and elemental composition of recent and fossil cyanobacteria, in *Astrobiology and Planetary Missions*, vol. 5906, p. 590603, International Society for Optics and Photonics.

Arp, G., A. Reimer, and J. Reitner (1999), Calcification in cyanobacterial biofilms of alkaline salt lakes, *European Journal of Phycology*, *34*(4), 393–403.

Batchelor, M., R. Burne, B. Henry, and M. Jackson (2004), A case for biotic morphogenesis of coniform stromatolites, *Physica A: Statistical Mechanics and its Applications*, *337*(1-2), 319–326.

Bedin, V., R. L. Adam, B. C. de Sá, G. Landman, and K. Metze (2010), Fractal dimension of chromatin is an independent prognostic factor for survival in melanoma, *BMC cancer*, *10*(1), 260.

Benning, L. G., V. Phoenix, N. Yee, and M. Tobin (2004), Molecular characterization of cyanobacterial silicification using synchrotron infrared micro-spectroscopy, *Geochimica et Cosmochimica Acta*, *68*(4), 729–741.

Berner, E. K., and R. A. Berner (2012), *Global Environment: Water, Air, and Geochemical Cycles*, Princeton University Press.

Berrendero, E., E. Perona, and P. Mateo (2008), Genetic and morphological characterization of Rivularia and Calothrix (Nostocales, Cyanobacteria) from running water, *International Journal of Systematic and Evolutionary Microbiology*, *58*(2), 447–460.

Brasier, M. D., and D. Wacey (2012), Fossils and astrobiology: new protocols for cell evolution in deep time, *International Journal of Astrobiology*, *11*(4), 217–228, doi: 10.1017/s1473550412000298.

Chappatte, D. (2010), Simulation of stromatolite growth using diffusion-limited aggregation and a discrete model of biogeochemical exchanges in microbial mat, Ph.D. thesis, Université de Lausanne, Faculté de biologie et médecine.

Cuerno, R., C. Escudero, J. García-Ruiz, and M. Herrero (2012), Pattern formation in stromatolites: insights from mathematical modelling, *Journal of the Royal Society Interface*, *9*(70), 1051–1062.

Donaldson, J. (1976), Aphebian stromatolites in canada: implications for stromatolite zonation, in *Developments in Sedimentology*, vol. 20, pp. 371–380, Elsevier.

Dupraz, C., R. Pattisina, and E. P. Verrecchia (2006), Translation of energy into morphology: Simulation of stromatolite morphospace using a stochastic model, *Sedimentary Geology*, *185*(3-4), 185–203, doi:10.1016/j.sedgeo.2005.12.012.

Dupraz, C., R. P. Reid, O. Braissant, A. W. Decho, R. S. Norman, and P. T. Visscher (2009), Processes of carbonate precipitation in modern microbial mats, *Earth-Science Reviews*, *96*(3), 141–162.

Farmer, J. D. (2000), Hydrothermal systems: doorways to early biosphere evolution, *GSA Today*, *10*(7), 1–9.

Feder, J. (1988), *Fractals*, 11, 34, 56 pp., Plenum Press.

Fouke, B. W. (2011), Hot-spring Systems Geobiology: abiotic and biotic influences on travertine formation at Mammoth Hot Springs, Yellowstone National Park, USA, *Sedimentology*, *58*(1), 170–219.

Fouke, B. W., J. D. Farmer, D. J. Des Marais, L. Pratt, N. C. Sturchio, P. C. Burns, and M. K. Discipulo (2000), Depositional facies and aqueous-solid geochemistry of travertine-depositing hot springs (Angel Terrace, Mammoth Hot Springs, Yellowstone National Park, USA), *Journal of Sedimentary Research*, *70*(3), 565–585.

Frederick, M. R., C. Kuttler, B. A. Hense, and H. J. Eberl (2011), A mathematical model of quorum sensing regulated EPS production in biofilm communities, *Theoretical Biology and Medical Modelling*, *8*(1), 8.

Grotzinger, J., S. Gupta, M. Malin, D. Rubin, J. Schieber, K. Siebach, D. Sumner, K. Stack, A. Vasavada, R. Arvidson, et al. (2015), Deposition, exhumation, and paleoclimate of an ancient lake deposit, Gale crater, Mars, *Science*, *350*(6257).

Grotzinger, J. P., and A. H. Knoll (1999), Stromatolites in Precambrian carbonates: Evolutionary mileposts or environmental dipsticks?, *Annual Review of Earth and Planetary Sciences*, *27*, 313–358, doi:10.1146/annurev.earth.27.1.313.

Grotzinger, J. P., and D. H. Rothman (1996), An abiotic model for stromatolite morphogenesis, *Nature*, *383*(6599), 423–425, doi:10.1038/383423a0.

Hagens, M., and J. Middelburg (2016), Attributing seasonal pH variability in surface ocean waters to governing factors, *Geophysical Research Letters*, *43*(24), 12–528.

Hofmann, H. (1994), Quantitative stromatolitology, *Journal of Paleontology*, *68*(4), 704–709.

Hugo, R. C., S. L. Cady, and W. Smythe (2011), The role of extracellular polymeric substances in the silicification of calothrix: evidence from microbial mat communities in hot springs at yellowstone national park, usa, *Geomicrobiology Journal*, *28*(8), 667–675.

Kardar, M., G. Parisi, and Y. C. Zhang (1986), Dynamic Scaling of Growing Interfaces, *Physical Review Letters*, *56*(9), 889–892, doi:10.1103/PhysRevLett.56.889.

Karperien, A. (1999–2013), FracLac for ImageJ, http://rsb.info.nih.gov/ij/plugins/fraclac/FLHelp/Introduction.htm, User's Manual.

Klafter, J., M. F. Shlesinger, and G. Zumofen (1996), Beyond brownian motion, *Physics today*, *49*(2), 33–39.

Klock, J.-H., A. Wieland, R. Seifert, and W. Michaelis (2007), Extracellular polymeric substances (eps) from cyanobacterial mats: characterisation and isolation method optimisation, *Marine Biology*, *152*(5), 1077–1085.

Mahaffy, P. R., C. R. Webster, S. K. Atreya, H. Franz, M. Wong, P. G. Conrad, D. Harpold, J. J. Jones, L. A. Leshin, H. Manning, et al. (2013), Abundance and isotopic composition of gases in the Martian atmosphere from the Curiosity rover, *Science*, *341*(6143), 263–266.

Mangold, N., G. Dromart, V. Ansan, F. Salese, M. G. Kleinhans, M. Massé, C. Quantin-Nataf, and K. M. Stack (2020), Fluvial regimes, morphometry, and age of Jezero crater paleolake inlet valleys and their exobiological significance for the 2020 Rover Mission Landing Site, *Astrobiology*.

McKay, D. S., E. K. Gibson, K. L. Thomas-Keprta, H. Vali, C. S. Romanek, S. J. Clemett, X. D. Chillier, C. R. Maechling, and R. N. Zare (1996), Search for past life on Mars: possible relic biogenic activity in Martian meteorite ALH84001, *Science*, *273*(5277), 924–930.

Mojzsis, S. J., G. Arrhenius, K. McKeegan, T. Harrison, A. Nutman, and C. Friend (1996), Evidence for life on Earth before 3,800 million years ago, *Nature*, *384*(6604), 55.

Neveu, M., L. E. Hays, M. A. Voytek, M. H. New, and M. D. Schulte (2018), The ladder of life detection, *Astrobiology*, *18*(11), 1375–1402.

Noffke, N., G. Gerdes, T. Klenke, and W. E. Krumbein (2001), Microbially induced sedimentary structures: a new category within the classification of primary sedimentary structures, *Journal of Sedimentary Research*, *71*(5), 649–656.

Norris, T. B., and R. Castenholz (2005), Effects of Environmental Stressors on Photosynthetic Microorganisms in Geothermal Springs of Yellowstone National Park, in *Geothermal biology and geochemistry in Yellowstone National Park: proceeding of the Thermal Biology Institute workshop, Yellowstone National Park, WY, October 2003*, p. 221, Montana State University Publications.

Plummer, L. N., and E. Busenberg (1982), The solubilities of calcite, aragonite and vaterite in co2-h2o solutions between 0 and 90 c, and an evaluation of the aqueous model for the system caco3-co2-h2o, *Geochimica et cosmochimica acta*, *46*(6), 1011–1040.

Rasband, W. S., et al. (1997), ImageJ.

Ruff, S. W., K. A. Campbell, M. J. Van Kranendonk, M. S. Rice, and J. D. Farmer (2020), The case for ancient hot springs in Gusev crater, Mars, *Astrobiology*, *20*(4), 475–499.

Schidlowski, M. (1988), A 3,800-million-year isotopic record of life from carbon in sedimentary rocks, *Nature*, *333*(6171), 313.

Self, C. A., and C. A. Hill (2003), How speleothems grow: an introduction to the ontogeny of cave minerals, *Journal of Cave and Karst Studies*, *65*(2), 130–151.

Smith Jr, T., G. Lange, and W. B. Marks (1996), Fractal methods and results in cellular morphology—dimensions, lacunarity and multifractals, *Journal of neuroscience methods*, *69*(2), 123–136.

Uher, B. (2007), Morphological characterization of three subaerial Calothrix species (Nostocales, Cyanobacteria).

Verrecchia, E. P. (1996), Morphometry of microstromatolites in calcrete laminar crusts and a fractal model of their growth, *Mathematical geology*, *28*(1), 87–109.

White, W. M. (2013), *Geochemistry*, John Wiley & Sons.

Yee, N., V. R. Phoenix, K. O. Konhauser, L. G. Benning, and F. G. Ferris (2003), The effect of cyanobacteria on silica precipitation at neutral ph: implications for bacterial silicification in geothermal hot springs, *Chemical Geology*, *199*(1-2), 83–90.

Appendix A: Chemistry

The equations governing calcite solubility are

$$CaCO_3 + H_2CO_3 \rightleftharpoons Ca^{2+} + 2\,HCO_3^- \qquad \text{(1.1 from section 1.2.2)}$$

and

$$CO_2 + H_2O \rightleftharpoons HCO_3^- + H^+ \rightleftharpoons CO_3^{2-} + 2\,H^+ \qquad \text{(1.2 from section 1.2.2)}$$

The chemistry leading to carboante stromatolites is ongoing: carbonate stromatolites formed billions of years ago and continue to form today. They form in diverse environments, each with their own conditions to be taken into consideration. This discussion of the chemistry of stromatolite formation will consider both ancient stromatolites forming as the first life on Earth developed and current stromatolites forming on a planet with well-established life.

A.1: Temperature and Pressure

Often, the relationship between temperature and solubility has a positive correlation, but calcite is actually more soluble at *lower* temperatures. *Plummer and Busenberg* [1982] conducted experiments on calcite, aragonite, and vaterite solubility at different temperatures in a CO_2/H_2O solution, so the reactions taking place include both those in eqs. 1.1 and 1.2. Their results show that all polymorphs of calcium carbonate are more soluble at lower temperatures (figure A.1).

Temperature controls in MISS-forming environments include solar and geothermal heating. In tidal environments, solar heating dominates. In shallow-sea environments, a combination of both direct solar heating and convection will influence local temperature. And in hot spring environments, geothermal heating will be the primary control, with temperatures being highest at the vent and lowest at the farthest reaches of the outflow channels.

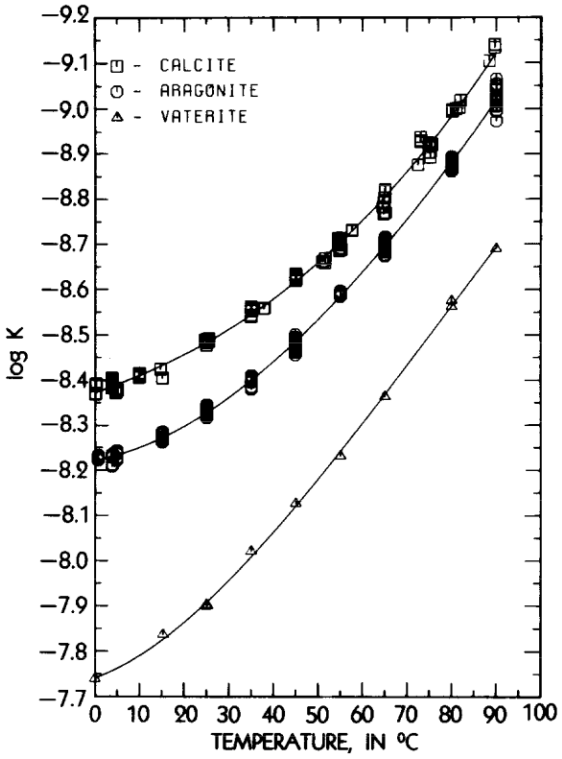

Figure A.1: Calcite, aragonite, and vaterite solubility as a function of temperature, from *Plummer and Busenberg* [1982].

In tidal environments and shallow sea environments, pressure can be expected to be fairly constant in still water. In hot springs, however, water is under higher pressure before it leaves the vent and rapidly loses pressure once it emerges. This causes rapid degassing of CO_2, which will drive eq. 1.2 to the left, driving 1.1 toward precipitation. The role of CO_2 will be discussed in more depth in section A.2.

A.2: Acidity

Acid dissolves calcite and carbonic acid is very common in MISS-forming environments, forming as CO_2 dissolves into water (eq. 1.2). Currently in shallow sea environments, the amount of dissolved CO_2 is increasing as CO_2 in the atmosphere increases, leading to ocean acidification, which drives 1.1 to the right.

CO_2 concentrations are highly dependent on the metabolisms of living organisms. Equation A.1 describes cellular respiration; equation A.2 describes photosynthesis.

$$C_6H_{12}O_6 + 6\,O_2 \longrightarrow 6\,CO_2 + 6\,H_2O + \text{energy (ATP)} \tag{A.1}$$

$$6\,CO_2 + 6\,H_2O + \text{energy (light)} \longrightarrow C_6H_{12}O_6 + 6\,O_2 \tag{A.2}$$

For the photosynthetic microbes that form MISS, the light-dependent photosynthesis cycles dominate during the day, taking up CO_2; at night, respiration dominates, releasing CO_2. So there is biologically forced diel cycling of CO_2 concentration, as illustrated in figure 1.2.

Finally, abiotic seasonal pH cycling occurs in the oceans. Some of this is the result of temperature changes: during the summer, the sun raises water temperature, which can cause CO_2 to come out of solution; in the winter, water radiates that heat into the atmosphere, which can allow CO_2 to dissolve. Temperature dominates the pH cycling at low and mid latitudes [*Hagens and Middelburg*, 2016], which could, hypothetically, lead to an entirely abiotically produced layered rock structure, if temperature changes are extreme enough (see figure A.2). However, such extreme temperature changes do not occur on Earth.

Other factors affecting seasonal pH cycling include atmospheric CO_2 concentrations and the amount of dissolved inorganic carbon (DIC) already in the environment. DIC dominates pH cycling at high latitudes [*Hagens and Middelburg*, 2016] and is strongly mediated by the metabolic processes already discussed. During the summer, photosynthetic algae in polar waters take in so much CO_2 that the pH rises, which can increase the rate of calcite precipitation.

In the hot springs used as the basis for this model, it is reasonable to ignore these cycles, both biotic and abiotic. The temperature of hot springs is primarily geothermally controlled, even

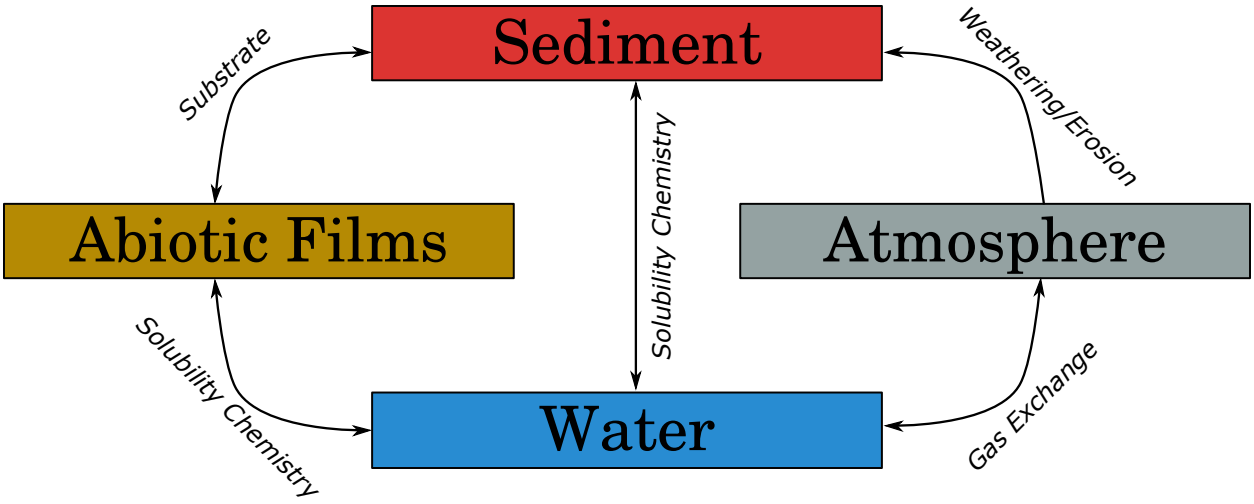

Figure A.2: An abiotic stromatolite system. Arrows point toward what is affected; for example, the atmosphere affects and produces sediment through weathering and erosion.

in the distal slope facies farther from the source, so abiotic CO_2 cycling can be ignored. That geothermal heating drives off a great deal of CO_2, keeping springs basic, which encourages calcite precipitation [*Fouke et al.*, 2000].

A.3: Ca^{2+} and Calcium Carbonate

In both ocean surface waters and travertine-depositing hot springs, water is either saturated or supersaturated with respect to calcium carbonate, meaning small changes in temperature, pressure, or concentrations of the species involved can induce precipitation.

Groundwater can become calcium-enriched as it passes through and dissolves limestone, dolomite, or plagioclase. Furthermore, oceanic Ca^{2+} concentrations can be increased at divergent boundaries: fresh basalt and seawater react to produce Ca^{2+} and the hot seawater convects and distributes that calcium *Berner and Berner* [2012]. So groundwater outflow into the ocean and tectonic activity are two ways to introduce calcium into seawater. In modern seas, shell-forming organisms act as a calcium sink; in Precambrian seas, these organisms had not yet evolved, leaving abiotic calcium carbonate precipitation to bring the system back to equilibrium.

Some microbial species produce EPS that interacts with calcium, so microbes can control calcium abundance. These species' EPS contain amino acids and polysaccharides that can bind Ca^{2+} to them; when that EPS is destroyed (by UV, acidity changes, or metabolic byproducts), it will release any bound Ca^{2+} [*Dupraz et al.*, 2009]. So EPS acts as a reservoir that can store and release calcium, acting as a sort of buffer. That reservoir can be overwhelmed with high enough alkalinity and enough evaporation, producing so many calcium ions that

all binding sites on the EPS become occupied and calcite precipitation can begin [*Arp et al.*, 1999]. However, the *Calothrix* at Yellowstone was not found to force precipitation of calcite [*Fouke et al.*, 2000]. This leaves only abiotic factors such as temperature, pressure change, and acidity to precipitate calcite in these systems.

Appendix B: Code Snippets

In addition to the snippets here, all the code and data that I am able to provide is available in full at https://github.com/bamcrunchbolt/stromatolites. This includes my additions to *DLA 3D EXT*, my R code, and my data. For the full *DLA 3D EXT* code, contact Dr. Eric Verrecchia at University of Lausanne. He was happy to share, but he wants to be in control of the sharing.

```
int InitialSurfaceManager::makeSpike(std::vector<char> &
    particlesField,
    InitialSurfaceSettings settings, int sizeBase, int sizeHeight
        , int sizeBaseSquare) {

  if (settings.spikeBottom==true){// start with bumpy surface
    makeRandom(particlesField, settings, sizeBase, sizeHeight,
        sizeBaseSquare);
  }else{// start with flat surface
    makeFlat(particlesField, sizeBaseSquare);
  }
  int x, y;
  int spikeHeight = settings.spikeFactor*sizeHeight*0.01f;
  if (settings.spikeField==true){//build spiike field
    for (int i=0; i<sizeBase; i++){
      if (i%settings.spikeSpacing==0){
        x = i;
      }
      for (int j=0; j<sizeBase; j++){
        if (j%settings.spikeSpacing==0){
          y=j;
        }
        for (int k=0; k<=spikeHeight; k++){
          particlesField[x + y*sizeBase + k*sizeBaseSquare] =
              NORMAL;
        }
      }
    }
  }else{//build single spike at center of starting surface
    x = sizeBase/2;
    for (int k=0; k<=spikeHeight; k++){
      particlesField[x + x*sizeBase + k*sizeBaseSquare] = NORMAL;
    }
```

```
  }
  return 0;
}
```

Listing B.1: Spike-creation code. Variables explained in the text (see section 2.2.1) are underlined.

```
run("8-bit");
run("Auto Threshold...", "method=Default white");
```

Listing B.2: Macro used to binarize images in ImageJ. "Default" means the isodata algorithm for thresholding images.

```
from random import random, randint
from math import sqrt

#Establish t limit, number of trials we want to do.
t = 1000000
numTrials = 10

# vertical movement down/up options --- same lengths, fortunately!
verticalMovementDown = [(1/3.+0/15.), (1/3.+1/15.), (1/3.+2/15.), (1/3.+3/15.), (1/3.+4/15.), (1/3.+5/15.), (1/3.+6/15.), (1/3.+7/15.), (1/3.+8/15.), (1/3.+9/15.), (1/3.+10/15.)]
verticalMovementUp = [((1+1/3.+0/15.)/2), ((1+1/3.+1/15.)/2), ((1+1/3.+2/15.)/2), ((1+1/3.+3/15.)/2), ((1+1/3.+4/15.)/2), ((1+1/3.+5/15.)/2), ((1+1/3.+6/15.)/2), ((1+1/3.+7/15.)/2), ((1+1/3.+8/15.)/2), ((1+1/3.+9/15.)/2), ((1+1/3.+10/15.)/2)]

# Open file for recording, write headers
f = open("motionTest1D_z.csv", "w+")
f.write("trial,MSD,t\n")
# Begin!
#pType = "xy" # set to "z" for z testing. Anything else defaults to x or y.
for j in range(0, numTrials):
  #reset all coordinates for the trial
  p = 0
  p2 = 0
  # Start the trial
  for i in range(1, t+1):
    if pType = "z": #if z motion, use z movement
      move = random()
```

```
      n = randint(0, len(verticalMovementDown)-1)
      if move < verticalMovementDown[n]:
        p -= 1
      elif move >= verticalMovementUp[n]:
        p += 1
    else: # else it's x or y motion, which is handled the same
      move = random()
      if move < 1/3.:
        p += 1
      elif move >= 2/3.:
        p -= 1
    p2 += p**2
    ## Calculate mean squared distance
    if i%1000 == 0:
      msd = float(p2)/i
      f.write(str(j+1) + "," + str(msd) + ","+ str(i) + "\n")

f.close()
```

Listing B.3: Python script to record the particle movement under the algorithm used in *DLA 3D EXT*.

Appendix C: Supplementary Figures

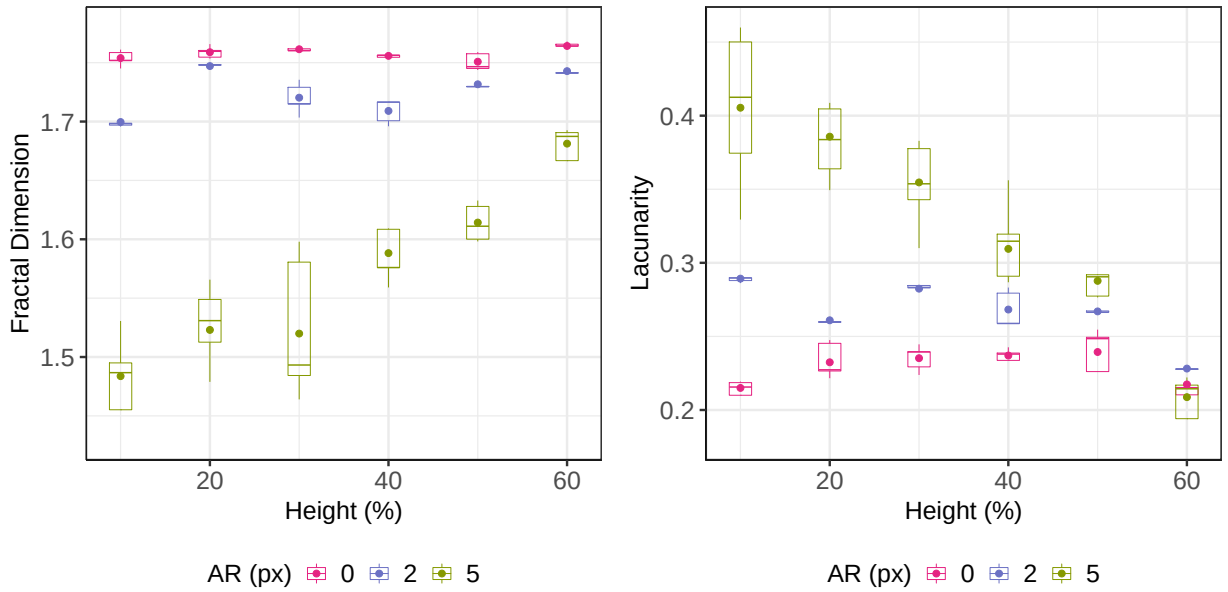

(a) **(b)**

Figure C.1: Fractal dimension (a) and lacunarity (b) of modeled stromatolites as a function of spike height. The height-morphology relationship is affected by changing AR initial conditions. When AR is high, morphology changes more with spike height.

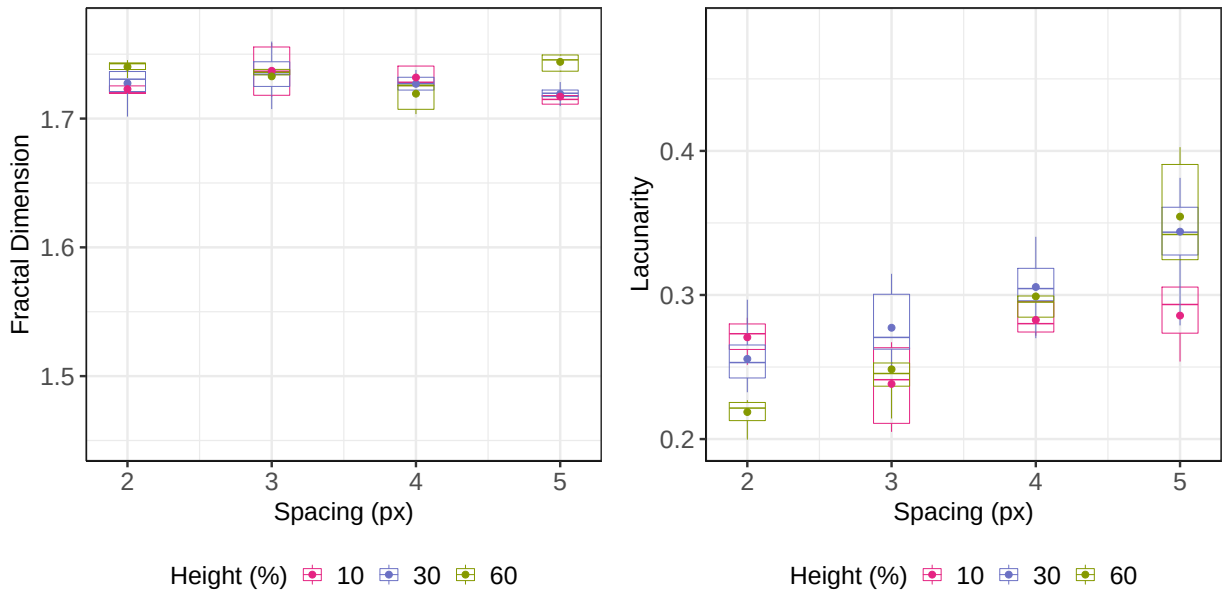

Figure C.2: Fractal dimension (a) and lacunarity (b) of modeled stromatolites as a function of spacing. The spacing-fractal dimension relationship is affected by changing height initial conditions; however, there does not seem to be any pattern produced by those changes. The spacing-lacunarity relationship is not affected by changing height initial conditions.